FOI
SWEDISH DEFENCE
RESEARCH AGENCY

FOI-R--0525--SE
June 2002
ISSN 1650-1942
Technical Report

Signal Processing Methods for Active Synthetic Aperture Sonar

Mattias Jönsson
Elias Parastates
Geoffrey Shippey
Jörgen Pihl
Peter Karlsson
Eva Dalberg
Bernt Nilsson

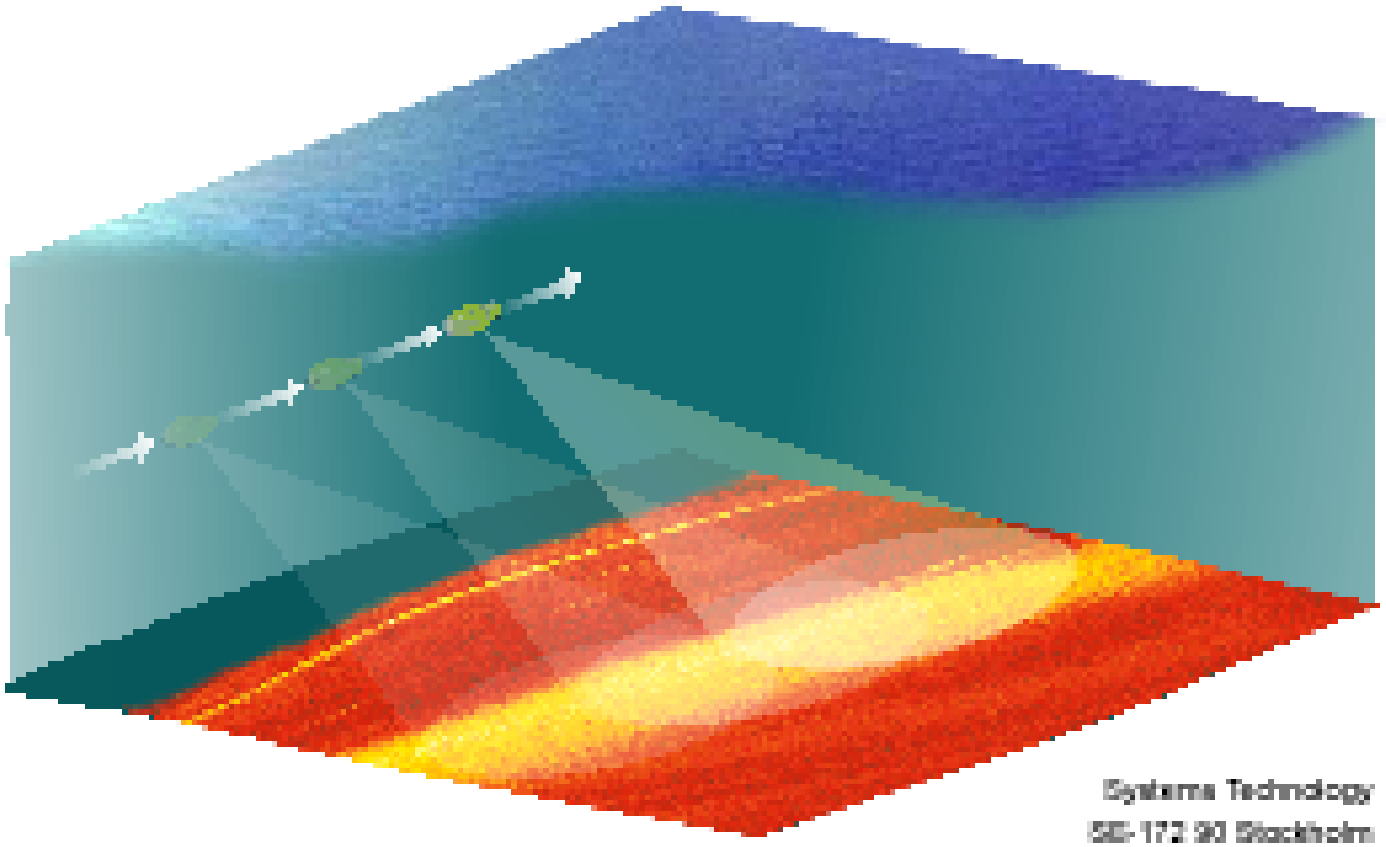

Systems Technology
SE-172 90 Stockholm

SWEDISH DEFENCE RESEARCH AGENCY
Systems Technology
SE-172 90 Stockholm
Sweden

FOI-R--0528--SE
June 2002
ISSN 1650-1942
Technical Report

Signal Processing Methods for Active Synthetic Aperture Sonar

Mattias Jönsson

Elias Parastates

Geoffrey Shippey

Jörgen Pihl

Peter Karlsson

Eva Dalberg

Bernt Nilsson

Issuing organization

FOI - Swedish Defence Research Agency
Systems Technology
SE-172 90 Stockholm
Sweden

Report number, ISRN
FOI-R--0528--SE

Report type
Technical Report

Research area code
4. C4ISR

Month year
June 2002

Project number
E6053

Customers code
5. Commissioned Research

Sub area code
43 Underwater Sensors

Author/s (editor/s)
Mattias Jönsson, Elias Parastates,
Geoffrey Shippey, Jörgen Pihl,
Peter Karlsson, Eva Dalberg, Bernt Nilsson

Project manager
Jörgen Pihl

Approved by

Sponsoring agency
Swedish Armed Forces

Scientifically and technically responsible
Mattias Jönsson

Report title

Signal Processing Methods for Active Synthetic Aperture Sonar

Abstract

In the autumn 2001 FOI carried out a field experiment at the Älvsnabben test site in the southern Stockholm archipelago. The aim of the experiment was to test Synthetic Aperture Sonar (SAS) algorithms developed at FOI during the last two years. These algorithms had previously been used to analyse data from an earlier experiment at the Djupviken test site with good results. The same equipment was used in both experiments, but with minor modifications to the transmitter.

Studies of the recorded data revealed several shortcomings in the experimental equipment and experimental mistakes which made the analysis very complicated. Most problems stemmed from the lack of a proper navigation instrument on the Remotely Operated Vehicle (ROV) carrying the sonar. There were also incompatibility problems with some of the rented equipment. Even though none of the runs were good some analysis was still possible. Autopositioning algorithms were extended to exploit Fast Factored Back Projection (FFBP) imaging. FFBP was originally developed at FOI for wideband Synthetic Aperture Radar (SAR).

We give a status report from the SAS research, as well as an introduction to SAS theory.

In combination with the previous Djupviken experiment, our conclusions from the Älvsnabben experiment are that the algorithms work well, but that the sonar and navigation systems must be upgraded. The report concludes with suggestions towards a system specification.

Keywords

SAS, Sonar, UUV, Autopositioning, Mindetection, FFBP, ROV, Autofocus

Further bibliographic information

Language English

ISSN 1650-1942

Pages 39

Price acc. to pricelist

Utgivare

Totalförsvarets Forskningsinstitut - FOI
Systemteknik
172 90 Stockholm

Rapportnummer, ISRN
FOI-R--0528--SE

Klassificering
Teknisk rapport

Forskningsområde
4. Spaning och ledning

Månad, år
Juni 2002

Projektnummer
E6053

Verksamhetsgren
5. Uppdragsfinansierad verksamhet

Delområde
43 Undervattenssensorer

Författare/redaktör

Mattias Jönsson, Elias Parastates,
Geoffrey Shippey, Jörgen Pihl,
Peter Karlsson, Eva Dalberg, Bernt Nilsson

Projektledare
Jörgen Pihl

Godkänd av

Uppdragsgivare/kundbeteckning
Försvarsmakten

Tekniskt och/eller vetenskapligt ansvarig
Mattias Jönsson

Rapportens titel (i översättning)

Signalbehandlingsmetoder för Aktiv Syntetisk Apertur Sonar

Sammanfattning

Hösten 2001 genomförde FOI ett fältförsök vid Älvsnabben i Stockholms södra skärgård. Syftet var att förbättra och testa de algoritmer och datorprogram för syntetiskapertursonar (SAS) som utvecklats vid FOI under de senaste två åren. Dessa program har framgångsrikt användts för att analysera data från ett tidigare experiment vid teststationen i Djupviken. Samma utrustning har använts vid de båda experimenten, dock med vissa smärre skillnader i sändarkonfigurationen.

Studier av de inspelade signalerna från Älvsnabbenförsöket visade på ett antal ofullkomligheter i experimentutrustningen och misstag under utförandet som gjorde analysen komplicerad. De flesta problemen uppstod på grund av att vår undervattensplattform saknar ett navigationsinstrument. Dessutom fungerade en del av den inhyrda utrustningen inte bra tillsammans med FOIs. Trots att ingen av körningarna var bra har ändå viss analys kunnat genomföras. Våra algoritmer för autopositionering har förbättrats så att de nu kan använda den snabbare Fast Factored Back Projection (FFBP) metoden för avbildning. FFBP är utsprungligen utvecklad vid FOI för bredbandiga radarsignaler.

Vi ger en lägesrapport från vår SAS-forskning, samt en liten introduktion till SAS teori.

Våra slutsatser från de båda fältförsöken vid Djupviken och Älvsnabben är att våra metoder fungerar bra, men vi behöver en passande sonar och ett riktigt navigationssystem för att kunna genomföra SAS-mätningar. Rapporten avslutas med en rekommendation till fortsatt arbete syftande till en systemspecifikation på SAS.

Nyckelord

SAS, Sonar, UUV, Autopositionering, Mindetektion, FFBP, ROV, Autofokus

Övriga bibliografiska uppgifter

Språk **Engelska**

ISSN 1650-1942

Antal sidor **39**

Distribution enligt missiv

Pris: enligt prislista

Contents

1. Introduction

The ability to detect and classify mines is important for naval operations, shipping and fishing. In the Baltic there are many dumpsites with ammunition from the two world wars, which are not yet cleared up [1].

The mine is a relatively cheap weapon, and can be cheaply deployed. For example it can be deployed secretly from fishing ships. Hence it is an ideal weapon in the asymmetric conflicts of today, where small paramilitary or terrorist organisations can threaten even large countries. Mine hunting and route clearance in peacetime must be done without endangering the personnel. The capability to detect and classify mines at safe distances is important. FOI is presently developing an ROV based system with a sonar which can classify mines by means of a novel technique called synthetic aperture sonar (SAS).

1.1 Earlier work at FOI

SAS research started at FOI in 1999 with a field experiment using the PLUMS ROV at the Djupviken test site in the Stockholm archipelago. This experiment was a collaboration with Lund Institute of Technology, Lund University (LTH), Chalmers University of Technology (CTH), Subvision AB and Bofors Underwater Systems AB [2]. A synthetic aperture of 9m was achieved, giving a resolution of 0.05m at a distance of 100m, see Figure 1.1.

The Djupviken environment is very different from that described in much of the SAS literature where seabed echoes are used for autopositioning. The seabed is fairly flat, gently shelving to deeper water at increasing sonar range. At these low incidence angles, there were no seabed echoes except at very short range. The targets stood out sharply against a background only slightly above receiver noise level.

In the absence of seabed echoes, it was not possible to autoposition on the seabed as described in the literature, and demonstrated in an earlier rail experiment at, LTH, using the same sonar system. Modified methods were required to exploit the strong echoes from isolated targets. As described in [3], two different autopositioning methods were used successfully. The first is Principle Point Positioning (PPP), based on the corresponding Synthetic Aperture Radar (SAR) technique. The second method, image correlation, successfully recovered the correct shape of track, even with no initial knowledge of speed or direction of motion.

However, beacon positioning also worked well at Djupviken, which meant that platform heading was known to within 1-2 mrad. Accurate knowledge of heading simplifies the problem considerably. The image correlation methods used DPCA's (Displaced Phase Centre Arrays) [4]. Here the physical receiver array is divided into a leading and trailing subarray, which in combination with the transmitter gives leading and trailing phase-centre arrays. For correlation purposes signals derived from the trailing phase centre array are correlated with signals derived from the leading phase-centre array from the previous pings. Subarray lengths are chosen to minimise the separation between these two arrays in the along-heading direction. This maximises correlation between echoes from a broadside target area. As a result, the phase-centre array may move forwards, backwards, or obliquely. However its expected movement can be computed from the navigation file, using the known change of heading between pings. Actual movement between DPCA's can be estimated by echo and image correlation. It is then straightforward to determine the ping-to-ping movement of the platform itself, and not just the movement of the DPCA.

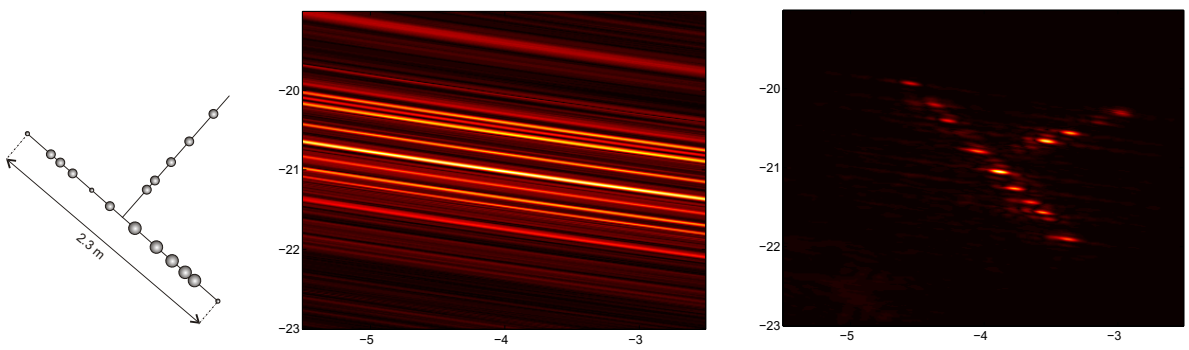

Figure 1.1: A test target made up by Styrofoam balls (left) depicted at 100 m distance with 0.5 m normal aperture sonar (middle) and 9 m synthetic aperture sonar (right).

1.2.The Älvsnabben experiment

The measurements at Djupviken were characterised by sonar signals with a low reverberation level. As a low reverberation level makes it easier to identify a target, we wanted to test our method in a less benign environment. A second experiment was therefore carried out at another site, the Älvsnabben site, which has a more complicated marine geology with rapidly varying bottom topography. This environment was carefully chosen to give strong echoes from the seabed. There were two main reasons for this. Firstly to investigate autopositioning on seabed echoes. Secondly, to verify whether autopositioning would still work if the background reverberation was higher. A steeply sloping side-wall of the bay was chosen to lay out the targets, with the further interest in investigating interferometric SAS.

1.3 Report layout

Most of the data from the Älvsnabben experiment has now been analysed. The results are presented in this report. Section 2 describes the methods used for SAS processing. A central problem in SAS is to determine the position of the sonar with sufficient accuracy. Hence much of the research has been devoted to find signal processing methods for determinining the movements of the ROV.

Section 3 reports on the Älvsnabben field experiment, with an overview of our equipment and a description of the test site. Our results from the measurements are presented in section 4. These results include side-scan images, measurements of the travel time variability, determination of ROV position and SAS images.

Finally, Section 5 gives some conclusions and suggestions for further research in SAS.

2. Method

2.1 Wideband SAS imaging

This section gives an introductory description of SAS image generation for engineers not specialized in the field. In order to prevent obstruction of the essential ideas in the image generation, the signal model and assumptions are strongly idealized, while preserving the central features needed for the addressed purpose.

2.1.1 The model of the sound pressure field

Consider a side looking sonar composed by a receiver antenna in the form of a Uniform Line Array (ULA) of elements and a transmitter antenna at some distance from the receiver. The sonar is carried on a platform, for instance a ROV (Remotely Operated Vehicle), moving at constant depth, at constant speed, along a straight track. The roll, pitch and yaw angles of the platform are constant throughout the track. The receiver antenna is in parallel to the track.

The transmitter sends a wideband pulse $u(t)$, of duration τ_S, with bandwidth $B >> 1/\tau_S$ centred about frequency f_c, at times $T = kT_S$, $k = 1,...,K$ where k and T_S denote the ping index and pulse repetition time respectively. The pulse is directed perpendicular to the platform, along the seabed. The azimuthal beamwidth of the transmitter allows sea-bed footprints of all pulses to overlap on a common frame, hereby termed as the image frame. Also the directivity in elevation is wide enough to insonify all seabed ranges of interest whilst avoiding insonification of the water surface.

Designate the world fix Cartesian coordinates for the projective centre of the transmitter by $\mathbf{r}_{\mathbf{T},k}$ and the receiver element by $\mathbf{r}_{\mathbf{R},k,l}$ where the receiver index $l = 1,...,L$.

Assume that pulses backscattered within the image frame and registered by the receivers can be modelled sufficiently well by a distribution of scatterers located at the coordinates $\mathbf{r}_{\mathbf{S},n}$, $n = 1,...,N$. The scatterer coordinates are constructed by division of the sea-bed area within the image frame into sub-areas, assigning one scatterer at the centre of each sub-area. In the idealized model we assume that the bathymetry is known, hence $\mathbf{r}_{\mathbf{S},n}$, $n = 1,...,N$ is also known.

The path delay for pulse k, between transmitter centre, scatterer and receiver configuration $\mathbf{r}_{\mathbf{T},k}$, $\mathbf{r}_{\mathbf{S},n}$ and $\mathbf{r}_{\mathbf{R},k,l}$, assuming a constant sound velocity c, is given by

$$\tau_{k,l,n} = \frac{\left\|\mathbf{r}_{\mathbf{S},n} - \mathbf{r}_{\mathbf{T},k}\right\| + \left\|\mathbf{r}_{\mathbf{R},k,l} - \mathbf{r}_{\mathbf{S},n}\right\|}{c}. \quad (1)$$

Approximate the backscattered pulse corresponding to that configuration by

$$a_{k,l,n}(t) = \begin{cases} p_{\mathbf{S},k,l,n}\, u(t-\tau_{k,l,n}), & |t-\tau_{k,l,n}| \le \tau_S/2 \\ 0 \text{ elsewere} \end{cases} \quad (2)$$

a time delayed copy of $u(t)$, scaled by $p_{\mathbf{S},k,l,n}$. Suppose that the Fourier spectrum of the pulse is symmetric about f_c. Then quadrature matched filtering [5, 6] of $a_{k,l,n}(t)$ using the replica

$$u_A(t) = u(t) + iH\{u(t)\} \quad (3)$$

where $H\{\ \}$ designates Hilbert transformation, yields

$$\int u_A(t'-t)a(t')dt' = \begin{cases} p_{\mathbf{S},k,l,n} u_C(t-\tau_{k,l,m,n}) e^{i2\pi f_c(t-\tau_{k,l,n})}, & |t-\tau_{k,l,n}| \le \tau_S \\ 0 \text{ elsewere} \end{cases} \quad (4)$$

.

The envelope $u_C(t-\tau_{k,l,n})$ of $\int u^*(t'-t)u(t'-\tau_{k,l,n})dt'$, where * denotes conjugation, has a main lobe within the time interval $|t-\tau_{k,l,n}| \le c/2B$. The analytic form of the sensor signal model after matched filtering is then

$$s_{\mathbf{R},k,l}(t) = \sum_{n=1}^{N} p_{\mathbf{S},k,l,n} u_C(t-\tau_{k,l,n}) e^{i2\pi f_c(t-\tau_{k,l,n})} \quad (5)$$

plus sensor noise.

2.1.2 Synthetic aperture processing

Synthetic aperture processing is a bistatic process involving the transmitter, the distribution of scatterers, and the receiver array. For many purposes, for instance the adaptation of standard SAR image reconstruction algorithms, it is convenient to replace this bistatic configuration by a monostatic configuration in which the ULA of the receiver elements is replaced by a ULA of phase centres [7] located approximately half-way between the transmitter and each receiver element. A ULA of receivers produces a nearly uniform ULA of phase centres, half the length of the receiver array.

We assume that the signals are registered with the platform moving with constant speed along a straight track and that they are matched filtered. To construct a synthetic aperture and focus on scatterer ν, begin by computing the two way time delays $\tau_{k,l,\nu}$ for the transmitter, scatterer and receiver coordinates $\mathbf{r}_{\mathbf{T},k}$, $\mathbf{r}_{\mathbf{S},\nu}$ and $\mathbf{r}_{\mathbf{R},k,l}, l = 1,...,L$, $k = 1,...,K$. Then, using (5), construct the matrix function

$$s_{\mathbf{R},k,l}\left(t+\tau_{k,l,\nu}\right) = p_{\mathbf{S},k,l,\nu}u_C\left(t\right)e^{i2\pi t} + \sum_{\substack{n=1\\ n\neq\nu}}^{M} p_{\mathbf{S},k,l,\nu}u_C\left(t-\tau_{k,l,n}+\tau_{k,l,\nu}\right)e^{i2\pi f_c\left(t-\tau_{k,l,n}+\tau_{k,l,\nu}\right)} \quad (7)$$

Notice that reverberation and noise terms, not appearing explicitly in (5), would add to the left hand side of equation 7.

Neighbouring columns in (6) overlap by q elements where q is defined as the value of the receiver index l that minimizes the distance $\left\|\mathbf{r}_{\mathbf{R},k+1,1}-\mathbf{r}_{\mathbf{R},k,l}\right\|_2$ between the trailing receiver element position $\mathbf{r}_{\mathbf{R},k+1,1}$ during pulse k+1 and the receiver positions $\mathbf{r}_{\mathbf{R},k,l}, l = 1,...,L$ during the previous pulse.

Suppose that the receiver element spacing is $\lambda_c = c/f_c$ and that L is an even number. If the array moves half the physical aperture $\|\mathbf{r}_{\mathbf{R},k,L}-\mathbf{r}_{\mathbf{R},k,1}\|_2/2$ between two consecutive pings, then the synthetic aperture should uniformly be filled by phase-centres spaced $\lambda_c/2$ apart which in turn avoid spatial alising and produces good

$$\mathbf{S}_\nu\left(t\right) = \begin{pmatrix} \ddots & 0 & & \\ & s_{\mathbf{R},k-1,1}\left(t+\tau_{k-1,1,\nu}\right) & & \\ & \vdots & & \\ & s_{\mathbf{R},k-1,l}\left(t+\tau_{k-1,q,\nu}\right) & 0 & \\ & s_{\mathbf{R},k-1,l+1}\left(t+\tau_{k-1,q+1,\nu}\right) & s_{\mathbf{R},k,1}\left(t+\tau_{k,1,\nu}\right) & \\ \ddots & \vdots & \vdots & \\ & s_{\mathbf{R},k-1,L}\left(t+\tau_{k-1,L,\nu}\right) & s_{\mathbf{R},k,l}\left(t+\tau_{k,q,\nu}\right) & 0 \\ & 0 & s_{\mathbf{R},k,l+1}\left(t+\tau_{k,q+1,\nu}\right) & s_{\mathbf{R},k-1,1}\left(t+\tau_{k+1,1,\nu}\right) \\ & & \vdots & \vdots \\ & & s_{\mathbf{R},k,L}\left(t+\tau_{k,L,\nu}\right) & s_{\mathbf{R},k-1,l}\left(t+\tau_{k+1,q,\nu}\right) \\ & & 0 & s_{\mathbf{R},k-1,l+1}\left(t+\tau_{k+1,q+1,\nu}\right) \\ & & & \vdots \\ & & & s_{\mathbf{R},k-1,L}\left(t+\tau_{k+1,L,\nu}\right) \\ & & & 0 \end{pmatrix} \quad (6)$$

$\in C^{L+q(K-1)\times K}$. The non-zero elements in column k are the receiver signals time shifted with delays that accounts for the propagation of pulse k along the paths pertaining to the transmitter, scatterer and receiver coordinates $\mathbf{r}_{\mathbf{T},k}$, $\mathbf{r}_{\mathbf{S},\nu}$, $\mathbf{r}_{\mathbf{R},k,l}, l = 1,...,L$. For instance element $\mathbf{S}_\nu\left(l+q(k-1),k,t\right)$ will be

SAS imagery. If for some reason (e.g. autopositioning, see Section 2.4) the platform moves less than half the physical receiver array length between adjacent pings, not all receiver elements are used for the SAS imaging.

The output of the synthetic aperture array is given

by

$$\bar{\gamma}_{\nu} = \int_{-\varepsilon c/2B}^{\varepsilon c/2B} \left| \mathbf{1}^T \mathbf{S}_{\nu}(t) \mathbf{1} \right| dt \tag{8}$$

where the integral is taken over a time corresponding to image resolution in the range direction, and $\mathbf{1}$ is a $L + q(K-1)$ vector with all elements set to one. Optionally, $\mathbf{1}^T$ may be substituted by a window function. $\bar{\gamma}_{\nu}$ is constituted by the sum of the elements in $\mathbf{S}(t)$ integrated over a small time interval. The travel time compensations bring echoes from pulses scattered at $\mathbf{r}_{\mathbf{s},\nu}$, in phase. These echoes are therefore reinforced by the summation, while the other terms are averaged out. In order to prevent influence from echoes due to neighbour scatterers, the integration interval is made small. In particular in this ideal case where the signal processing perfectly accounts for the pulse propagation and scattering, the integration interval may contain only a single sample.

2.1.3 Image creation

An image is created as follows:

1. Define a frame for the image over a part of the bottom surface that has been illuminated by pulses $k = 1,\ldots,K$
2. Divide the frame in N pixels (resolution cells).
3. To each pixel, assign one point scatterer with x,y coordinates determined by the geometric centre of the pixel and z coordinate given by the corresponding depth.
4. Compute the complete synthetic aperture array output for each pixel.

In practice the recorded sensor signals are sampled, with a sampling rate above the Nyquist frequency. Subsample signal interpolation, needed for the computation of the beamformed array output can be carried out by a computationally efficient method described in [6].

The method described above is known as “classical back-projection”, widely used for physical aperture radar and sonar imaging. However, the computational load becomes excessive for SAR and SAS imaging, unless N is small. For this reason a variety of Fourier-based methods have been developed within the SAR community [8]. Unfortunately these methods are difficult to apply to a multi-element receiver configuration, and also place limitations on track shape, bandwidth etc. Both objections are overcomed by the Fast-Factored Back Projection algorithm developed by FOI [9] for SAR. This is an approximation method which avoids the problem of having to include all phase-centres in combination with all pixels in the calculations. The iterative algorithm begins with all required echoes along the aperture and an image consisting of a single pixel spanning the whole frame. Then each pixel in the image is subdivided into more pixels as the echoes are successively combined into beams from fewer phase-centres. The process stops when the image reaches the required resolution and only one phase-centre remains. This method has been implemented for SAS and successfully been used to generate images from the Djupviken and Älvsnabben experiments.

SAS image creation as described above assumes an accurately known track. In the real world the platform is disturbed by various forces and water currents. As the SAS process is extremely sensitive (consider (7), with random errors in $\tau_{k,l,\nu}$) to deviation from the assumed track it is crucial that the true platform movements and orientations are registered with high precision to avoid performance degradation.

In the situation with known, isolated targets, the deviation between actual and registered platform movement and orientation be inferred from the non-zero elements in

$$\bar{\bar{\Gamma}}_{\nu}(\boldsymbol{\tau}, k) = \int_{-c/2B}^{c/2B} \mathbf{S}_{\nu}^{*}(t+\tau,:,k)\mathbf{S}_{\nu}(t,:,k+1)dt \quad , \quad k = 1,\ldots,K-1 \tag{9}$$

where : designates a matrix column.

2.2 Software calibration

The ultra-wide bandwidth of the receiver array used in the experiments (50-500 kHz) was obtained at the expense of variation between the transfer function of the individual transducer channels. To compensate for this a software calibration [10, 11] of the received echoes is performed. In this calibration multipath effects from reflecting boundaries on the receiver platform as well as amplitude and phase differences between the receiver elements may be reduced. In essence, the software calibration is a way to equalise distortions introduced by receiver elements.

In a calibration experiment the receiver array is placed at some distance from the transmitter. The transmitter emits the signal that will be used in the SAS processing measurements, and the received signal at every receiver is recorded. The received signals are then processed to produce a kernel set which is used to equalise the received signals after match-filtering. In this section the calibration procedure using the recorded pings is described. It is divided into several subsections; waveform recovery, pre-processing, deskewing, defocusing, channel equalisation and a check of the produced kernel set.

2.2.1 Waveform recovery

Very short time duration sine wave pulses may be used to estimate the system transfer function. A longer, and thus more energetic, wideband pulse would be advantageous, but this has the side effect of mixing the direct path with the multipaths. The waveform recovery step is optional in the calibration procedure, but in principle the system transfer function for each transmission channel may be estimated from the responses to the short pulses. The system transfer function may then be inverted and the emitted signal waveform recovered. However, waveform recovery is not normally a part of the calibration procedure.

2.2.2 Pre-processing

Pre-processing consists mainly of the selection of an appropriate section of the ping recorded by the middle receiver element. This signal is termed the mid-element replica. The corresponding section is then extracted from all the received signals, thus forming a matrix with received echoes. The extracted signals $S_{\mathbf{R},l}(t)$ $l = 1,..., L$ are then quadrature match-filtered, with the mid-element replica $S_{\mathbf{R},\lambda}(t)$ (cf. equation 4). The resulting complex correlation function is here denoted by $\Psi_{S_{\mathbf{R},l},S_{\mathbf{R},\lambda}}(t)$.

2.2.3 Deskewing and defocusing

In an experimental calibration the source and the receivers must not be separated more than a certain distance depending on the water depth at the calibration site. Or rather it is the distance from the source and the receivers to any reflecting surface in the vicinity that must be large enough. This is in order to separate the direct path signal from any multipath signals, giving a cleaner replica signal for use in subsequent processing.

An example is in order. Assume the transmitted pulse is 1 ms long. In order to get a clean direct path replica, no multipath signals must arrive at the receivers earlier than 1 ms after direct path arrival. A 1 ms time difference of arrival translates into a range difference of about 1.5 m. In a calibration experiment the source and the receivers were placed in the middle (3 m) of the water column (6 m). Using a source receiver separation of 10 m the path differences between the direct path and the bottom and surface reflected paths were 1.6 m, and thus the direct path signal was not contaminated by multipath signals.

Because the transmitter source and receiver array must be sufficiently close to separate multipath the wavefront will not be plane when it reaches the receiver array. As we would like to calibrate our array for far field signals a defocusing action is required. Here the effect of the spherical wavefront is removed. At the same time an incidence angle other than normal to the array may be corrected. This process is called deskewing.

Deskewing and defocusing are accomplished using an iterative MUSIC [12] algorithm. The initial value, β_0, for the iteration, a first estimate of the Direction Of Arrival (DOA), β, is established using linear regression, where a straight line is fitted to the measured arrival times over the receiver. The slope, *s*, of the straight line, expressed in samples per channel, and the inter-sensor distance, d_s, also expressed in samples, are calculated. Finally the DOA is computed using

$$\beta_0 = \sin^{-1}(s / d_s) \tag{10}$$

The data are now deskewed and defocused using the iterative MUSIC process, which is outlined with the pseudo-algorithm below:

1. Set $\hat{\beta} = \pi/4$, $\beta = \beta_0$ and M = 500.
2. Align received data using β.
3. Compute covariance matrix for aligned data.
4. Correct the inter-sensor distance for alignment.
5. Compute the MUSIC spectrum at M points on the interval $\left(-\hat{\beta}, \hat{\beta}\right)$.
6. Estimate $d\beta$ from the MUSIC spectrum.
7. Set $\beta := \beta + d\beta$.
8. Compute the range from the transmitter to every receiver using the new value of β.
9. Align data using computed ranges.
10. Set $\hat{\beta} := \hat{\beta}/2$.
11. Return to 3 if the maximum number of iterations is not yet reached.

Thus the deskewing and defocusing algorithm provides an aligned set of data over the receiver array.

2.2.4 Channel equalization

Now that the received signals are properly aligned the gain differences between receiver channels may be corrected. The aligned signals are match-filtered with themselves and the maximum of the absolute value is established for all channels. The received aligned signals, $S_{\mathbf{R},l}(t)$, are then scaled by the square root of these maximum values, respectively:

$$Z_{\mathbf{R},l}(t) = \frac{S_{\mathbf{R},l}(t)}{\sqrt{\max_t \left| \Psi_{S_{\mathbf{R},l}, S_{\mathbf{R},l}}(t) \right|}} \tag{11}$$

In effect this normalises the energy contained in all signals.

A Chebyshev window [13] is used to weigh the matched filter output of the normalised and aligned signals, $Z_{\mathbf{R},l}(t)$, with themselves into a single weighted response

$$\overline{Z}(t) = \frac{\sum_{l=1}^{L} w(l) \Psi_{Z_{\mathbf{R},l}, Z_{\mathbf{R},l}}(t)}{\sum_{l=1}^{L} w(l)} \tag{12}$$

where $w(l)$ are the Chebyshev weights. Instead of inverting for the emitted signal, we let $\overline{Z}(t)$ constitute the desired response and construct inverse filters for every channel that produce this desired signal. This is done in the frequency domain, yielding the kernel

$$k_l(t) = F^{-1}\left\{ \frac{F\{\overline{Z}(t)\}}{F\{Z_{\mathbf{R},l}(t)\}} \right\} \tag{13}$$

where $F\{\ \}$ denotes a Fourier transformation. Care must be taken in the above operation, as zeros in the denominator will produce poles in the resulting kernel. As $F\{\overline{Z}(t)\}$ is essentially the square of $F\{Z_{\mathbf{R},l}(t)\}$, it will take on small values in approximately the same areas and hence we may set $F\{\overline{Z}(t)\}$ to zero here. This is also correct in the sense that we have poor information about the channel in these frequency regions. The resulting kernel set is then reversed in time for use in subsequent matched filtering of pulse echoes.

2.2.5 Calibration check

Echoes obtained from other pings during the calibration may now be used together with the established kernel set. Thus a polar image of the transmitter may be created and inspected. If the beampattern and the range response are acceptable, the kernel set is saved and stored for subsequent processing.

2.3 Beacon positioning

Platform position can be determined by measuring range and incidence angle to transmitters, called “beacons”, mounted on the seabed. The matched-filtered signal is first windowed to remove any surface or bottom reflection. This should also eliminate signals from other sources. The platform moves at a slow steady speed, so the window is chosen around the range determined from the previous ping.

Look angle is determined by MUSIC. Range can be determined by measuring signal travel time from the peak amplitude of the compressed signal. The MUSIC look-angle allows beamforming in the beacon direction and range can be estimated from the beam. Accuracy is increased by interpolating the signal ten times.

Estimations of range and DOA (direction of arrival) are made in a plane containing the beacon and the receiver array. This plane will be different for each platform position. Useful positioning must be made in the same coordinate system for each ping. Range and look-angle are therefore resolved into the horizontal plane. If slant range is R_s, slant look angle θ_s, pitch η_s and the depth difference between the transmitter and the beacon Z are according to [11], then the look angle

$$\Theta_h = \arctan\left(\frac{Y}{X}\right) \tag{14}$$

and the horizontal range

$$R_h = \sqrt{X^2 + Y^2} \tag{15}$$

where

$$X = \frac{R_s \sin(\theta_s)}{\cos(\eta)} + Z\tan(\eta), \tag{16}$$

$$Y = \sqrt{R_s{}^2 \cos(\theta_s)^2 - \frac{(Z + R_s \sin(\theta_s)\sin(\eta))^2}{\cos(\eta)^2}}. \tag{17}$$

Platform position can be determined from the horizontal ranges and angles to two beacons. Consider the coordinate system defined by the two beacons and having its origin midway between them. The x-axis is aligned with the line between the beacons and the y-axis is pointing at right angles to the x-axis towards the platform. The platform position in this coordinate system can be determined by simple trigonometry. First consider the scene in Figure 2.1.

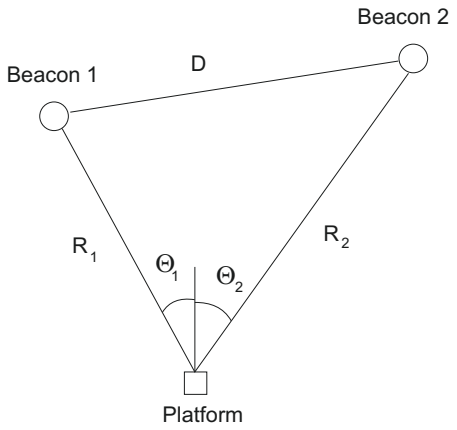

Figure 2.1: The platform and two beacons projected on a horizontal plane.

The separation between the beacons D is determined from the law of cosines

$$D^2 = R_1{}^2 + R_2{}^2 - 2R_1R_2\cos(\theta_1 + \theta_2) \tag{18}$$

Separation between the beacons is estimated as the mean separation over all pings.

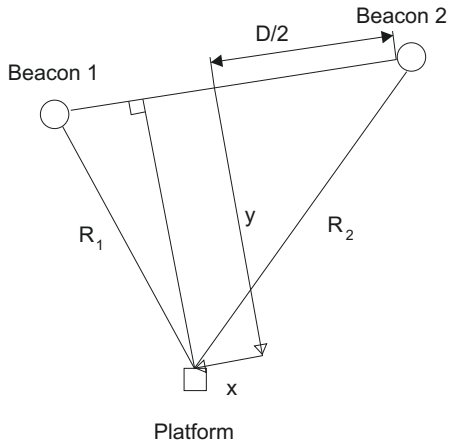

Figure 2.2: The platform, the beacons and the beacon coordinate system.

From Figure 2.2:

$$(x + D/2)^2 + y^2 = R_2^{\,2}, \tag{19}$$

$$(x - D/2)^2 + y^2 = R_1^{\,2}, \tag{20}$$

giving

$$x = \frac{R_2^{\,2} - R_1^{\,2}}{2D}, \tag{21}$$

$$y = \sqrt{\frac{R_1^{\,2} + R_2^{\,2}}{2} - \frac{D^2}{4} - x^2} \quad . \tag{22}$$

The heading, h, for the platform, is defined positive anti-clockwise from the x-axis in the beacon coordinate system, see Figure 2.3. It is calculated for both beacons and the true heading is taken as the mean value.

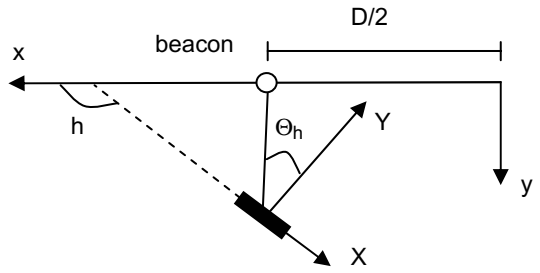

Figure 2.3. Schematic over the heading definition.

From Figure 2.3 the heading is given by the relation

$$h = \arctan\left(\frac{y}{x - D/2}\right) + \Theta_h + \frac{\pi}{2} \quad . \tag{23}$$

The basic positioning problem is to find the point where estimated ranges to two fixed beacons agree. If the beacons are close together compared to the range to the vehicle, then the x-coordinate is more affected by errors in range estimates than the y-coordinate. However, if the beacons are far apart the y-coordinate is more affected by errors in range estimates than the x-coordinate. How much the y-coordinate is affected by range errors also depends on vehicle position. When the vehicle moves towards the x-axis the y-coordinate becomes more affected by errors. Very close to the x-axis a small range estimation error will cause a large position error. Unless the aim is to increase accuracy in one coordinate the ideal configuration is an equilateral triangle.

Alternatively the platform position can be determined with only one beacon from a known starting position, using the change in azimuth angle, between pings, to obtain the track. These polar angles, $d\theta$, are found with the help of either platform speed or change in heading together with incidence angle. From the velocity the angles are given by

$$d\theta_{k+1} \approx \frac{\sqrt{(vdt)^2 - (r_{k+1} - r_k)^2}}{r_k} \tag{24}$$

where *v* is the velocity, *dt* the time between the pings, r_k and r_{k+1} are the ranges between the platform and the beacon at ping *k* and *k+1*.

If heading information is used instead the azimuth angle is found as the sum of the difference in incidence angles, $\theta_{k+1} - \theta_k$, and the change in heading, dh_{k+1},

$$d\theta_{k+1} = \theta_{k+1} - \theta_k + dh_{k+1} \, . \tag{25}$$

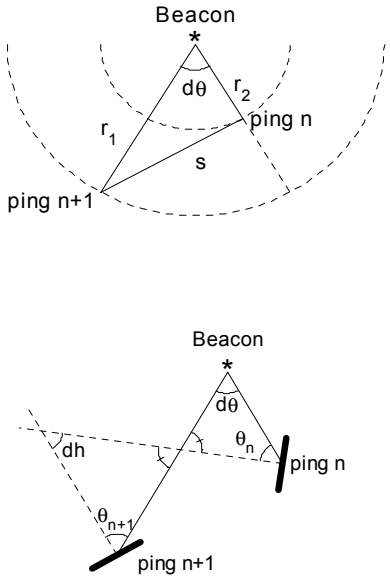

Figure 2.4. Geometry schematic for calculating the change in azimuth angle for two consecutive pings. The left panel displays the mean speed approach and the right the incidence-heading method.

The Cartesian coordinates for ping *k+1* are now given as a function of the position of the previous ping, the current range and angle,

$$x_{k+1} = r_{k+1}\cos\left(\tan^{-1}\left(\frac{y_k}{x_k}\right) + d\theta_{k+1}\right) \quad (26)$$

$$y_{k+1} = r_{k+1}\sin\left(\tan^{-1}\left(\frac{y_k}{x_k}\right) + d\theta_{k+1}\right) \quad (27)$$

where the origin for the Cartesian coordinate system is chosen at the beacon position.

If heading is required instead of the polar angle, (24) and (25) give the change in heading, which (when knowing the starting heading) can be summed to the current heading, as

$$dh_{k+1} \approx \frac{\sqrt{(vdt)^2 - \left(r_{k+1} - r_k\right)^2}}{r_k} - \left(\theta_{k+1} - \theta_k\right). \quad (28)$$

2.4 Autopositioning by Echo and Image Correlation

2.4.1 Introduction

Generation of a SAS image requires a very accurate estimate of the track followed by the sonar platform along the length of the synthetic aperture. For satellite-borne Synthetic-Aperture Radar, it may be sufficient to assume a straight track. For airborne SAR, some corrections to this straight-track assumption are usually necessary. A number of "autofocus" methods have been developed for SAR in which the radar echoes are used to determine track curvature.

For a platform moving slowly through a water medium, the perturbations to the track are much more severe, and one ore two curvature parameters are inadequate to describe this perturbation. A good estimate of heading is also important for SAS imaging, so heading error can be included in this track perturbation. The word "autopositioning" is used here to describe some method of correcting the assumed track using the sonar echoes themselves. This section will summarise a set of DPCA methods in which platform corrections are made by correlating echoes or images derived from successive pings.

For many purposes it is useful to correlate echoes or images of random scatterer distributions on the seabed. If the platform moves half the receiver array length between pings, as required by SAS sampling theory, then echoes from successive pings become totally decorrelated. This gave rise to the DPCA methodology. Using the DPCA method, the transmitter or receiver array is moved electronically backwards between successive pings as the platform moves physically forward, so that the phase-centre array remains nearly stationary in the along-track direction. If this condition is satisfied, then echoes from random distributions of reflectors on the seabed or target objects remain highly correlated. It is then possible to estimate the displacement between the arrays in the direction of the mean echo DOA, and use this information to correct the navigation file. This initial navigation file may be computed using an INS (Inertial Navigation System) or other dead-reckoning system. Alternatively it may be computed with the aid of acoustic beacons (Section 2.3). If no information is available from either source, one can begin by assuming a straight track with constant heading at some guessed platform speed through the water.

2.4.2 Technical Background

Estimation of Time Displacement by Wideband Correlation

All wideband processing is carried out using quadrature match-filtered echoes. Under certain assumptions [6] the quadrature match-filtered echo of a chirp pulse from a point reflector is just the compressed envelope modulating a complex carrier signal at mid-frequency. The time displacement between two sampled wideband echoes can now be found by correlating the match-filtered echoes, in a manner similar to narrowband interferometry. The time displacement is found to the nearest sample by the location of the peak amplitude of the correlogram, while the sub-sample time-displacement is given by the phase at this peak. Time displacements can be converted to distance using the assumed speed of sound.

The sonar configuration

The methods and software reported below are designed for a sonar configuration with one transmitter array, so DPCA's are created by choosing leading and trailing subsets from the same receiver array. The experimental receiver array contained 32 transducer channels spaced by 15mm. This generates a 32-channel phase-centre array with 7.5mm spacing. The number of elements used for each DPCA array depends on platform speed. For example a platform speed of 10.5 cm/ping corresponds to a forward movement of 14 phase-centres/ping, so 14–element displacement is needed between the two phase-centre subarrays. This can be achieved using a leading subarray consisting of elements 1-19, and a trailing subarray with elements 14-32. The faster the platform speed, the shorter the DPCA's become. Finally at a platform speed of ½ array length/ping, the DPCA length vanishes, so the method becomes unusable.

For each ping along the sonar track, the three platform position coordinates (x, y, z) and heading, pitch and roll angles (Φ, η, ρ), are stored in a *navigation file*. (z, η, ρ) values are obtained from the platform recorder, and need to be synchronized with the echo data, and smoothed to remove quantization steps. Initial (x, y, Φ)values are obtained either by beacon positioning or by guesstimate. The task of autopositioning is to correct errors in these values leading to phase incoherence in the along-bearing direction to the target, or angle errors in the cross-bearing direction.

It simplifies autopositioning to use a coordinate system in which the x-axis is aligned with mean heading. The receiver boresight should then point close to the y-axis for most of the track. It is also convenient to place the origin at the centre of the track for the ping-sequence of interest. This coordinate system will be termed *track coordinates*. If the original navigation file is derived in beacon coordinates, it is rotated into track coordinates before autopositioning begins.

The echoes from the seabed used for autopositioning are chosen within a certain range bracket from the sonar platform. Echoes from the seabed within this range bracket will have a mean elevation angle. The autopositiong programs estimate differences between propagation times to the DPCA's from this region of seabed. All time estimates are carried out in the plane containing the DPC Array and the selected region of seabed. It is convenient to rotate the navigation file into this tilted plane before autopositioning begins.

Wideband Beam-Forming

Autopositioning is carried out using beamformed echoes. The beamforming code is adapted from the code used elsewhere for SAS imaging. Beamforming is carried out towards an image reference point in 3D space, from an array of phase-centre locations whose 3D positions can be derived from the existing navigation file. Phase-centre locations are generated routinely for each ping using the platform position and attitude given in the navigation file, and the defined image reference point.

Beamforming uses the *timetable* function in the FFBP SAS code [9]. This function computes the propagation time from each phase-centre location to an array of pixel centres. Echo segments are then aligned by clipping and phase-shifting so that echo delays to the centre sample equal the computed propagation times. As in SAS imaging, phase-shifting at mid-frequency is used to implement sub-sample time-delays. The required beam is then a weighted sum of the aligned echoes, using standard Chebycheff aperture shading functions. A conceptual by-product of beamforming is a virtual array of phase-centres normal to the beam direction. Correlation of two beamformed echoes gives the displacement between these virtual arrays.

Intermediate FFBP Images

Correlating a set of echoes in a fixed direction can only give the navigation error in that direction. To estimate navigation errors in two dimensions, it is necessary to correlate echoes from a range of directions. The original FOI image correlation code, and the image correlation code described in [14] used "conventional" sonar images with one complex value for each pixel location. The current code uses intermediate FFBP images, which are not images at all in the ordinary sense. The intermediate FFBP image is a set of beamformed echo segments segmented and phase-shifted so that the number of samples in the segment spans the pixel, while the centre sample corresponds to the required value at the pixel centre.

The FFBP images" used in *autoimage* are generally rather sparse, e.g. 27x3 pixels. This leaves segments long enough for good correlation, e.g. 1000 samples. Each segment radiates out from the centre of the DPCA towards the pixel location on the seabed, and contains precisely the values needed for correlation in the pixel direction.

Program Overview

The autopositioning suite consists of four programs:

autoecho_SS (Sidescan Autoecho)

autoecho-FF (Fixed Frame Autoecho)

autoimage-SS (Sidescan Autoimage)

autoimage-FF (Fixed Frame Autoimage)

The two ***autoecho*** programs are closely related, and correlate beam-formed sonar echoes from successive pings. The two ***autoimage*** programs are also closely related, and correlate FFBP images generated from successive pings.

Navigation Corrections

After running *autoimage* the navigation file is updated using the program

newnav = navcompxy(oldnav,xerror,yerror,nstart,nstop);

After running *autoecho* the navigation file is updated using the program

newnav = navcompxyphi(oldnav,xerror,yerror,psi,nstart,nstop);

xerror, yerror, psi are estimated ping-to-ping errors in (x, y, Φ) using a convention that the error is the true value minus the given value. Hence estimated errors are subtracted from the values given in *oldnav* to make the required correction. Both programs sum the given errors from pings *nstart* to *nstop* and subtract mean values before carrying out the update. All programs determine navigation errors in the *along-bearing* and *across-bearing* directions. These errors are then resolved into track coordinates in order to correct the navigation file. This step is redundant for the two sidescan programs where the bearing direction is always the y-axis.

2.4.3 Echo Correlation Programs

Autoecho-SS

This program is derived from a method developed by Belletino and Pinto at the SACLANT Centre [15], which is itself derived from a method described by Sherriff [7]. Figure 2.5 illustrates a pair of overlapping DPCA arrays looking at the seabed broadside of the sonar platform. In Belletino and Pinto, transmission is synchronized with platform movement estimated by an INS. It is therefore possible to achieve very accurate stabilization of array displacement against platform movement. Individual transducer echoes can then be correlated successfully. Correlation of echoes from corresponding channels gives a set of displacements versus channel location along the phase-centre axis. Mean displacement gives the lateral displacement of the DPCA between pings (sway), whereas displacement slope gives DPCA rotation between pings.

Unless transmission is accurately synchronized with platform movement, the displacement between corresponding channels can easily exceed the transducer dimensions. This leads to total baseline decorrelation. Moreover the echo DOA is poorly defined by an individual transducer element with low directivity. If the scanned seabed contains geological structures such as rock outcrops or target objects, the mean echo DOA could easily deviate from broadside, leading to sway estimation error.

Pulse transmission was not synchronized with platform movement in the FOI experimental sonar system. In fact the speed of the platform over the seabed could only be guessed in most of the Älvsnabben experiments. To achieve echo correlation under these circumstances,

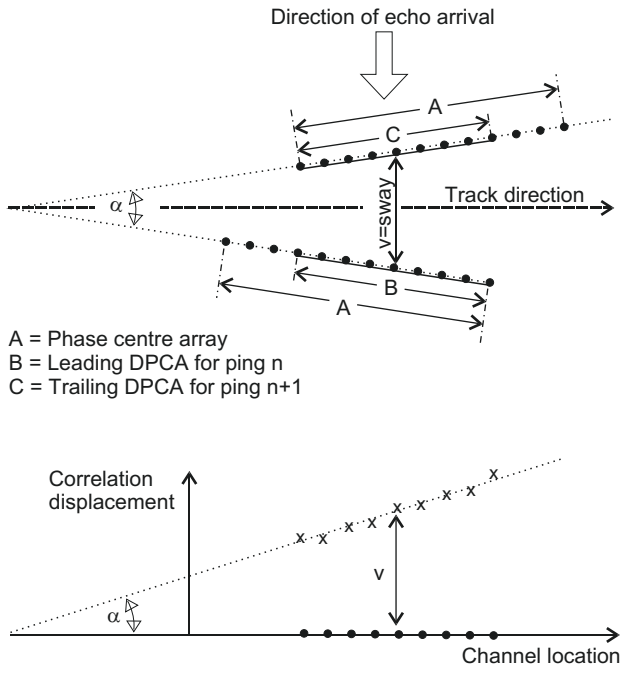

Figure 2.5: DPCA Sway and Heading Estimation

individual phase-centre elements are grouped into overlapping subsets. For example an 18 channel DPCA could be grouped into the ten clusters 1:9, 2:10, 3:11, … 10:18. Echoes belonging to each subset are then beamformed in the *y*-direction. Corresponding beams from successive pings are used to derive the corresponding values as in Belletino and Pinto. This strategy has two advantages. Firstly correlation is preserved against phase-centre displacement by using longer subarrays. Secondly the directivity of each subset can be used to select echoes with a chosen DOA.

As described in Belletini and Pinto, the complete echo within a selected range bracket is used for correlation purposes. In the FOI implementation, the echoes are divided into shorter overlapping segments. This increases correlation levels wherever stronger reflectors are encountered by the sonar beam.

The beamforming code automatically takes account of heading change predicted by the navigation file, so the output from the program is not change of heading between pings, but the error in change of heading.

Autoecho_FF

The Belletino and Pinto method take no account of along-track errors. This is justified by the assumption that the target of interest is broadside to the centre of the synthetic aperture and only small look-angles are involved. In these circumstances, SAS phase coherence depends mainly on cross-track navigation accuracy, since only a small component of along-track navigation error is resolved towards the target. Whether or not this argument applies to an operational sonar, it certainly did not apply to the situation in the Djupviken and Älvsnabben experiments. Therefore, consider a variant of the first method in which autopositioning is carried out using echoes from an area of seabed containing the target or close to the target. A fixed frame is used to define the required echo range and direction, and this frame does not move with the platform (Figure 2.6). The code used for *autoecho_FF* is almost the same as autoech_SS, since receiver directivity is already implemented.

However, the analysis is different. Autopositioning on the target area itself has two desirable properties:

i) Navigation error is measured along the line of sight to the target area, termed the “along-bearing displacement”. This is the important direction for SAS phase-coherence.

ii) Correlation slope now depends on unpredicted cross-bearing motion of the platform as well as unpredicted change of heading. Heading is then corrected in such a way that the target lies in the required direction, even when the along-track motion given in the navigation file is itself wrong.

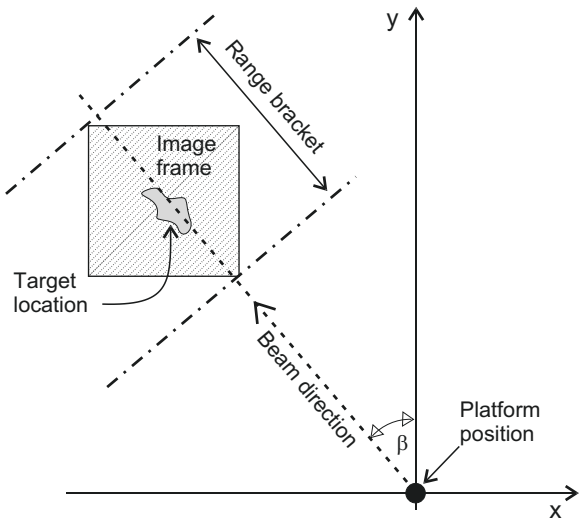

Figure 2.6: Fixed Frame Echo Correlation.

However, the corrected navigation file can only be used for the selected area, since the corrections are useful but not "true".

2.4.4 Image Correlation Programs

The ***autoecho*** programs correct the navigation file in one specific direction. It would be useful to determine both components of track error, i.e. along-heading and cross-heading. It would then be possible to form a phase-coherent SAS image of any part of the scene using the same navigation file.

autoimage_SS correlates FFBP physical-aperture images of the seabed scanned by the sonar platform as it moves along its track. These images are generated from same DPCA's used for autoecho. If each DPCA contains 18 channels, then all 18 channels are used to form each image.

autoimage_FF correlates FFBP images of a fixed area of seabed.

The angle subtended by the image frame in azimuth should be wider than the azimuth resolution of the physical aperture images. Otherwise no cross-bearing information is obtained. To understand the program principle, consider a simplifed example. Figure 2.7 shows a 3x3 pixel image frame. The image is generated in (X,Y) track-coordinates, but shown in bearing coordinates (U,V), so the image frame is rotated in the diagram. Each DPCA image consists of nine beamformed echo segments. Image correlation involves the pairwise correlation of these nine segments.

If DPCA movement is small and there is no navigation error, the imaging code compensates for platform movement and attitude change, so the images should coincide. Hence correlation will detect no systematic displacement between corresponding segments. However if the ping-to-ping navigation errors along the U and V axes are (g,h) the displacement between corresponding segments will correspond to (g,h) resolved in the direction of the pixel centre, i.e.

$$d = -g\sin(\gamma) + h\cos(\gamma) \tag{29}$$

where γ is the bearing angle shown in the diagram. Given nine estimates of d, and nine known values of γ it is straightforward to find the least-square error estimate. Since echoes from some pixels are stronger than other, and correlation levels also vary, it is desirable to weight the least-squares fit with some combination of cross-power and cross-correlation.

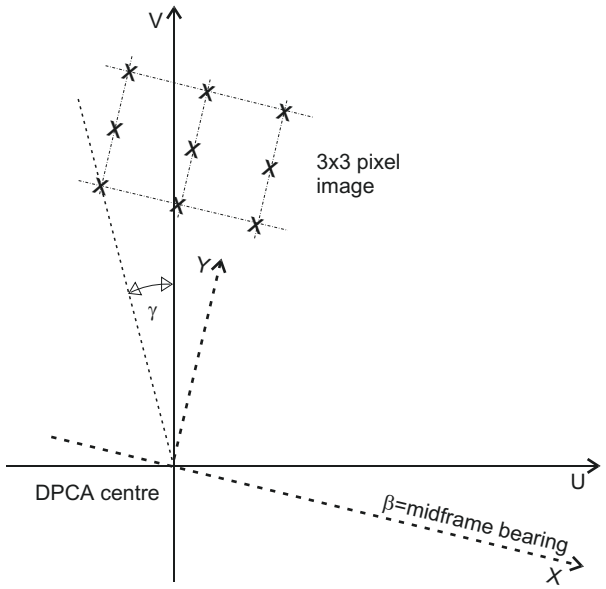

Figure 2.7: Autoimage Geometry.

The above analysis assumes that samples in each echo segment are reflected from the seabed within each pixel area. If one dominant reflector is present in the scene, this assumption will not hold. The image is then dominated by one point-spread function spanning the whole image. This point-spread function rotates as the platform moves around the target area. It can be shown that the g value no longer corresponds to cross-bearing navigation error, but to cross-bearing movement of the platform. Hence autoimage_ff can only be used where the reflector model is very clear.

2.4.5 Interdependance of Track Errors and Heading Error

autoecho and ***autoimage*** each estimate errors in two of the three parameters (x, y, Φ). These errors are interdependent, so the navigation file cannot just be updated using each program in turn. The first step in improving the updating procedure is to look at the interdependence between the incremental errors, (g, h, ψ).

ψ *and* (g,h)

The correlation programs estimate the displacement of the DPCA subarrays between pings, and compare this to the displacement predicted from the navigation file. For SAS imaging, we require the motion of the complete array, not the DPCA subarrays.

As shown in Figure 2.8 leading and trailing DPCA's for the same ping are separated by distance L along the phase-centre axis. The centre of the full array lies midway between them, and it is convenient to take this as the platform reference point. Consider a sequence of two pings. Figure 2.8 shows the leading DPCA for ping 1. The axis lies at angle θ with respect to the midframe bearing.

For ping 2, the array has rotated through a small additional angle α according to the navigation file, but actually through $\alpha+\psi$. Also:

i) DPCA centre displacement between pings = (u,v) in the along/across-bearing directions according to the navigation file, but $(u+g, v+h)$ as estimated by autopositioning.

ii) The autopositioning programs allow for heading rotation α in computing but not ψ .

It can be seen by simple geometry that the additional along-bearing displacement of the reference point = $L\psi$ in a direction normal to the DPCA's. Hence the estimated displacement errors (g,h) need to be modified to

$$(g',h')=(g-L\psi\sin(\theta), h-L\psi\cos(\theta)) \qquad (30)$$

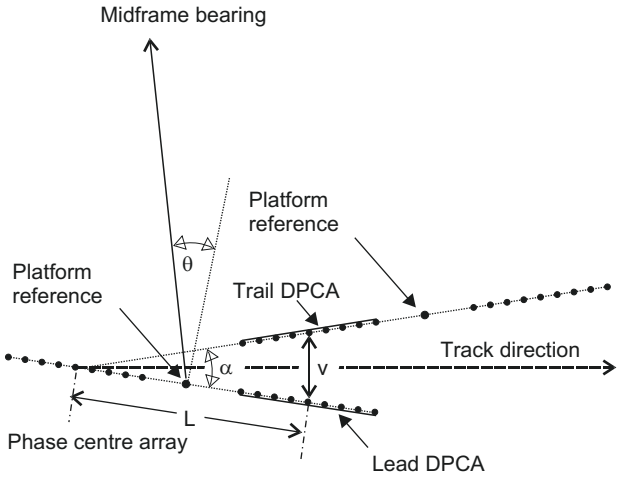

Figure 2.8: Heading Error Geometry.

g *and* ψ

The error estimate ψ allows for predicted platform motion in the cross-bearing direction, but not for the cross-bearing motion error, g. Hence ψ should be adjusted to

$$\psi' = \psi - g/R \qquad (31)$$

where R is slant range to midframe. From (30) and (31)

$$\psi' = \psi - g/R + L\psi\sin(\theta/R) \qquad (32)$$

In our experiments, L/R was of order 10^{-3} so the third term is negligible. ψ' can now be used in equation (31) to adjust *g* and h .

Hence it does not seem too difficult to allow for incremental error interdependence. Unfortunately this does not solve the problem completely:

- Both *autoecho* and *autoimage* compute phase-centre locations using the existing navigation file. These phase-centre locations depend on the summed heading angle Φ .
- Beam-steering in *autoecho* also depends on ϕ.
- Incorrect values of Φ lead to incorrect resolution of along- and across-bearing errors into track coordinates.

For all these reasons the estimated errors depend on the summed heading error, and not just the incremental heading error, ψ . To allow for this, the navigation file must be updated for all previous pings before correcting platform position for the next ping. To preserve the policy that navigation corrections average out to zero, processing should start in the middle of the aperture, and work forwards and backwards towards the ends. These modifications involve no fundamental changes to the current algorithms, but a significant amount of programming.

In the absence of such a program, the three parameter autopositioning problem has been solved by running *autoecho* and *autoimage* iteratively and in turn. This procedure converges, even without correcting for incremental error interdependence as shown above. Convergence is slow, but this may be due to neglecting dependence between incremental errors.

2.4.6 The reflector model

At the acoustic frequencies used, the surficial seabed sediment can be modelled as a random distribution of individual reflectors with dimensions of the order of the acoustic wavelength. It is less obvious that man-made targets can be modelled in the same way, but in fact this model is often used for detection and imaging purposes.

autoecho_ss is sensitive to strongly reflecting off-boresight seabed structures, since these perturb the mean echo DOA away from boresight. Belletino and Pinto assume a flat seabed without geological structure containing a uniform random distribution of fine reflectors. This also excludes man-made targets. Such an environment is seldom encountered. Beamforming used in the FOI code should reduce the problem, but will not eliminate it. Hence it is undesirable to select a sidescan swath which contains strong targets.

autoecho_ff is more tolerant of seabed structures, and the image frame can actually be centred on a point-like target. This is a further advantage of this program.

The two *autoimage* programs are much more tolerant of a non-uniform seabed containing geological structures or target objects. The only requirement is that useful echoes are generated across the image area. If *autoimage_ff* is used with a small image frame containing one dominant reflector, this requirement is not satisfied.

2.4.7 Parameter Estimation

Navigation error estimation is a two-stage process – correlation of available echo sets, followed by parameter extraction.

Correlation

Each pair of corresponding match-filtered echo-segments is correlated to give the following parameters:

1. Peak correlation level.
2. Echo displacement, computed from the peak location and phase at the peak.
3. Ratio of peak correlation to next highest correlogram peak.
4. Cross-power.

The correlation is rejected unless parameters 1 and 3 exceed some preset threshold, and parameter 2 lies below some threshold. The correlation function outputs rejection statistics on the screen to help the operator adjust threshold values where necessary. The correlation function outputs three array displacements, peaks of Cross Correlation Functions (CCF) and cross-powers.

Weighting

Cross-power and peak CCF values are very variable. At Älvsnabben the image area often spanned a region of seabed with changing level of insonification. Hence some weighting function should be applied to each displacement value for purposes of parameter extraction. The weighting chosen at the moment is $\sqrt{\text{crosspower} * \text{peak CCF}}$. However this weighting function has never been optimised.

Ambiguity Adjustment

Parameter extraction from the displacement array presents considerable problems. Both ½λ ambiguities and outliers are frequently encountered, and sometimes few good displacement values are available from the correlation function. The Belletino and Pinto reference considers only errors due to Guassian receiver noise. Using the FOI experimental system, more severe problems are due to:

1. Channel inequality
2. Baseline decorrelation
3. Inadequate bandwidth

These factors need proper investigation when circumstances permit.

Displacement ambiguities are adjusted in both programs using an *ambiguity-check* algorithm. This computes the weighted standard deviation for the whole set of displacements, and the change to this sd caused by ½λ shifts of each displacement value in turn. The displacement value giving the biggest standard deviation reduction is then adjusted by some multiple of ½λ . This process is repeated until no further reduction in standard deviation is achieved.

Slope and mean shift extraction for autoecho

These parameters can be extracted by a weighted least-square error line fit. However, this least-squares fit is sensitive to outliers, so it is preceded by outlier elimination. A weighted Hough transform is used to find the dominant lineation in the data. If no dominant lineation is found, then the least-squares fit line is used. The standard deviation of all displacements in the dataset from this line is computed. Any displacement exceeding this standard deviation by more than a given factor is deemed an outlier and removed. The process is repeated until no more outliers are identified. The final step is a weighted least-squares fit.

g and h extraction for autoimage

The procedure is similar, except that the aim is a best fit to the displacement dataset of the form

$$d_n = -g\sin(\gamma_n) + h\cos(\gamma_n) \tag{33}$$

where each displacement value d_n is weighted by w_n. It is straightforward to find (g,h) by weighted least-squares fit. Outliers are removed by clustering the values in a similar way to the Hough transform. A range of g values is selected, giving a corresponding h value for each point in the dataset. These (g,h) points are then mapped in space. As with the Hough transform a strong cluster of points indicates the required linear solution.

2.4.8 Discussion

This section has described the autopositioning programs used to process the Djupviken and Älvsnabben data. Discussion has been simplified by assuming a flat seabed. In practice, variable seabed topography poses additional problems which have not been discussed. The principle of displaced phase centre echo correlation is well documented in the literature. However we believe that the adaptation of this principle in the FOI programs is novel. The programs have been used to find three unknown parameters in experimental data, starting from a guessed straight track with constant heading. Currently, processing is very slow. The problem is simplified considerably if heading angle is known – at least well enough to remove systematic errors. The programs have been developed to handle the difficult experimental data. Hopefully these difficulties will not be representative for operational equipment.

3 Field experiments

3.1 Equipment

The field experiments use several systems which must work well together for the experiment to be successful. The main components are:

- The ROV
- Transmitters and receiver.
- A high-speed digital recorder.
- Auxiliary hydrophones for positioning and monitoring.
- Signal generators and amplifiers.
- CTD-meter for measurement of the water sound speed profile.

The ROV used for the Djupviken and Älvsnabben was an old system, PLUMS (Platform for Underwater Measurement Systems) developed at FOA in 1986-1987 (Figure 3.1).

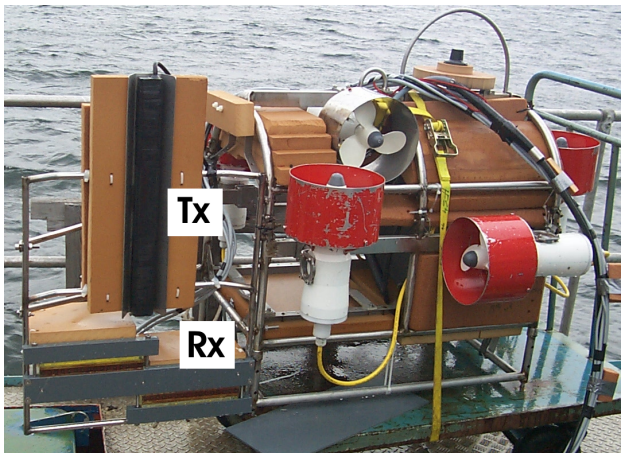

Figure 3.1 The PLUMS (Platform for Underwater Measurement Systems) with the vertical transmitter array and horizontal receiver array (here split in two halves for interferometric reception).

PLUMS can be operated down to maximum depth of 100 m. Heading, roll and pitch angles can be set with a precision of about one degree. The relative accuracy is 0.1 degree. PLUMS is controlled by an on-board computer, which reads the outputs from a gyro, two tilt meters, a compass and a depth gauge. The on-board computer communicates over a serial link to the on-shore computer for operator control of the vehicle. This Windows-based program presents the PLUMS data in a convenient user interface (Figure 3.2). The program also logs all data from PLUMS for further processing.

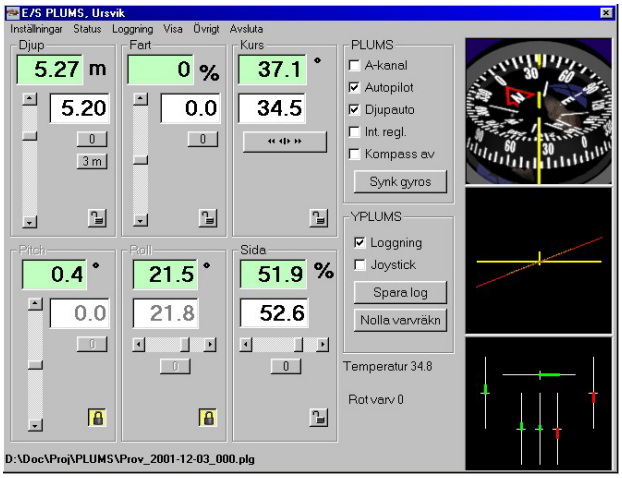

Figure 3.2 The operator´s interface to the PLUMS control system. The operator selects values for depth, speed, roll etc. by a joystick or the mouse (digits on white background). Actual values are shown with green background. The right hand panel shows heading (the compass, at the top), roll and pitch (in the middle) and motor thrusts (lower).

In the experiments a vertically mounted side-scan array was used as the sonar transmitter with a nominal one degree vertical beamwidth. This was shaded to increase the effective beamwidth to 4.2 degrees. The operating centre frequency was 100 kHz. The purpose of employing this side-scan array was to use its narrow beam to avoid surface reflections. The receiver array was part of a system developed at LTH, called DAIM (Digital Acoustic IMaging). The linear array consists of two 16-element hydrophones arrays. When mounted side by side they form a 32-element array with a total length of 0.5 m.

The high-speed data recorder (part of the DAIM system) contains 32 one-board data acquisition systems coupled in parallel. Each system can record data on an internal disc with a speed of up to 2 Msample/s. Hence the total maximum system capacity is 64 Msamples/s. In the experiments the system was operated at 312.5 – 2000 ksamples/s per channel.

The two auxiliary hydrophones acting as acoustic beacons were similar to those used for positioning in the Djupviken experiment. Monitoring hydrophones where placed at two of the targets to help adjust the roll angle of PLUMS to insonify the target area (Figure 3.4-5).

3.2 Environment

The measurements were performed in a semi-enclosed bay in the Stockholm Archipelago in October 2001. The bay has a varied bathymetry and the experiments were conducted on a steep slope. In order to select a suitable site for the experiment, the bay was previously surveyed by side-scan sonar at a frequency of 100 kHz. The sea-floor at the test site is covered by so called gyttja-clay, a soft post-glacial clay and mud, which constitutes a rather inhomogeneous layer. At shallow depths, less than around ten metres, the top soft deposit is thin. This is probably a result of the ordinary eroding swell of the shallower parts. The eroded particles are transported away from the relatively steep slopes and deposited on deeper water. The seabed surface is smooth and without vegetation below a few metres depth. On the seabed there is a lot of litter deposited, such as logs and anthropogenic artefacts. As in other parts of the Stockholm Archipelago, below the uppermost clay there is a thin layer of till, typically some metres thick. The bedrock consists mainly of crystalline granites, gneisses and leptites formed about 1800 Ma ago.

In the experimental area, roughly 50x60 m^2, the depth varied from 15-25 m. The targets were placed in the shallower parts of the area, with the ROV carrying the transmitter/receiver-system operated in the deeper parts. The ROV was steered from “Skotten”, a barge-like working platform approximately 12x4 m^2 in size. This platform also carried the electronics for the transmission and data acquisition systems.

Four different objects were arranged in a row, spaced by five meters. The two beacons were placed at each end of the row, ten metres away and five meters in front of the objects. Figure 3.3 shows an overview of the experimental area. The targets were an ordinary house-hold ladder equipped with a reference hydrophone (Figure 3.4), two rectangular objects of size of 1x1.5 m, and the so-called T-target (Figure 3.5). The T-target consists of a T-formed metal frame with plastic foam balls attached on short rods above it. This target also had a reference hydrophone mounted.

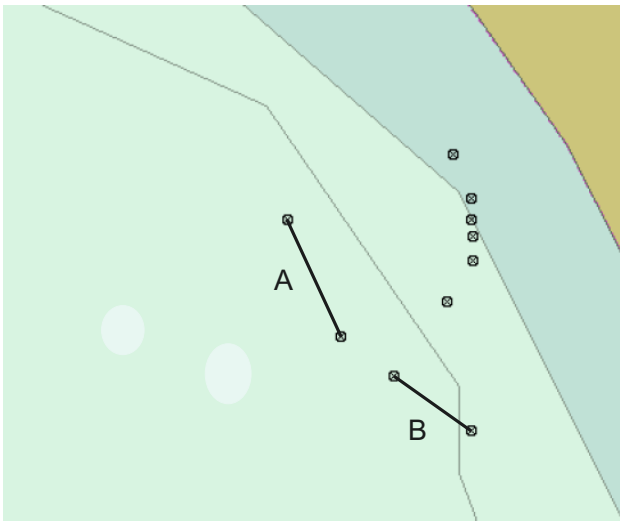

Figure 3.3: The experimental area. A and B denotes the two tracks used

Figure 3.4: The step target with a monitor hydrophone.

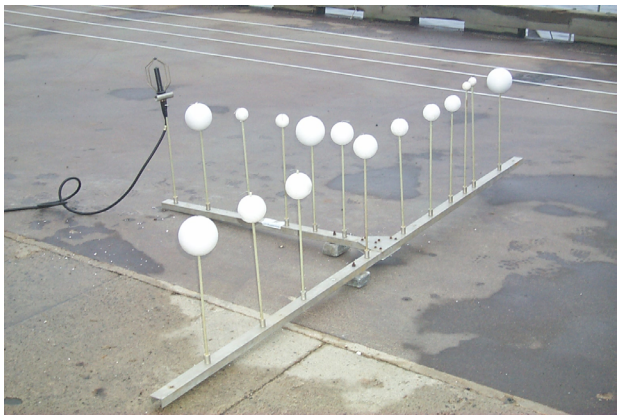

Figure 3.5: The T-target with a monitor hydrophone.

Sound speed profiles were recorded at three occasions during the measurements. No dramatic changes occurred during the experiment days, as Figure 3.6 illustrates. However, the positioning resolution required for successful use of the SAS algorithm is such that even a small change of sound speed motivates the use of a positioning method which does not depend on separate measurements of the sound speed profile.

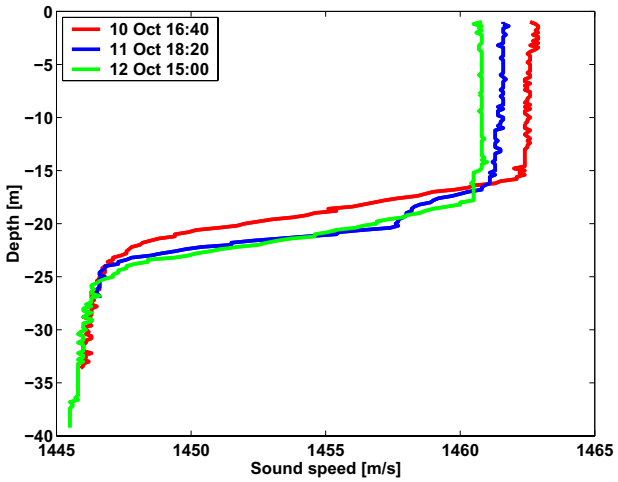

Figure 3.6: Sound speed profiles recorded at three occasions during the experiments.

3.3 Activities

Three different pulses were used for imaging. The first signal was a linear chirp between 90kHz and 110kHz with an M formed frequency pattern. The receiver array has a narrow resonant peak at 100 kHz. The M-form should then give a flatter frequency pattern after reception. Secondly a pulse that consists of three consecutive chirps amplitude modulated by a fourth chirp was used. The amplitude modulation generates a parametric low frequency chirp. The chirps are chosen around the transmitter resonant peaks. The chirps are 91-107kHz, 329-345kHz and 556-572kHz. The parametric effect should give a chirp between 3kHz and 19kHz. Finally the linear chirp from 60kHz to 120kHz previously used in the Djupviken experiments was used again. The two receiver arrays were mounted in two different configurations. Firstly side by side to form a long 32-element array. Secondly vertically separated to be able to make interferometric or 3D images. In order to image the targets from different directions, two alternative tracks were used for the PLUMS vehicle. At the first location three runs were carried out, one for each pulse. Here the receiver arrays were mounted side by side. These runs will be termed ”LAM”, ”LAP” and ”LAW” where M denotes the M-formed pulse, P the signal with the parametric effect and W the signal with the widest frequency pattern. At the second location two runs were carried out, one for each receiver configuration. The M-pulse was used in both experiments. The runs will be termed LBM and IBM where L denotes linear array and I interferometric configuration.

Since new signals and new sampling frequencies were used, preliminary experiments were required to record replicas. A calibration experiment for each signal was therefore conducted. Normally broadside replicas are preferred. However the receiver array has internal reflections so large that it is also useful to record replicas at larger incident angles.

4. Results

4.1 Preprocessing

Apart from the equipment problems referred to earlier, the experiments were also affected by a misunderstanding that was not discovered until it was too late. The divers placed the targets and beacons wrongly with respect to the selected tracks for PLUMS. With our limited equipment this was disastrous. The narrow transmitter elevation beamwidth means that the transmitter must point in almost exactly the right direction to illuminate the targets properly. Obviously this is very difficult when the targets are somewhere else. Mispositioning of the beacons introduced another problem. For half of the runs the track crossed the extension of the line between the two beacons. Beacon triangulation breaks down in this situation. To handle this situation a method for positioning on one beacon was developed. The experience from Djupviken suggested a straightforward plan for processing: calibration, beacon positioning, SAS imaging and improved SAS imaging using autopositioning. However, this plan was quickly abandoned. Here every run had to be examined thoroughly to determine what was possible to achieve from each run. Processing went back and forth between quality control, positioning and search for targets by imaging as one problem after another was revealed.

By considering missing pings, effective bandwidth, target illumination, beacon signals, track location and synchronisation between the two recording system the LBM and LAP experiments were chosen to be processed. Neither of them looked good but the others seemed to have even more problems. In the LBM run only one beacon was visible so 1-beacon positioning methods had to be developed and tested. LAP had two visible beacons and turned out to be a good experiment for comparing the new methods with 2-beacon positioning. Simultaneously autopositioning revealed a synchronisation error between the platform clock and the sonar system clock. This was also confirmed by beacon positioning. The two different approaches of 1-beacon positioning then turned out to solve the positioning and synchronisation problems together. The less accurate mean velocity method was used to solve the synchronisation error and the more accurate heading method was then used to determine the track. Even though positioning was possible targets were hard to find. Sidescan images revealed no targets. The wrongly located LBM track meant that only one target was illuminated. The LAP experiment, initially for testing a new pulse form, had only recorded data up to 50m range. This meant that three targets were only illuminated at the beginning of the track using very large look angles. Worse still, the platform speed was unacceptably high for SAS processing.

4.1.1 Quality control

For all processing there are some basic requirements. Here the final goal is SAS images but to be able to do that positioning is needed. Therefore the basic requirements for both positioning and imaging have to be considered, including the following aspects.

Missing pings: Sometimes the DAIM system fails to record a ping. When a ping is missing the autopositioning algorithm may fail since the platform moves more than the expected distance between the recorded pings.

Effective Bandwidth: The range resolution is determined by the bandwidth. Both transmitter and receiver have frequency dependent beampatterns. Obviously the effective bandwidth does not have to be the same as the nominal bandwidth.

Illuminated targets: The transmitter beamwidth is very narrow in elevation. All targets may not be illuminated if the roll angle of the ROV is wrong, or the pitch angle is excessive.

Beacon signals: To be able to do beacon positioning the beacons must transmit as desired and be identifiable in recorded data.

Track location: Beacon positioning accuracy depends on track location. As discussed above PLUMS crossed the x-axis for several runs breaking down triangulation.

Synchronization error: The recording system and the platform navigation system are independent with different sampling frequencies. Time for both systems are also recorded and used to synchronize the data. However there is evidence that the clocks were unsynchronised (Sections 4.1.4 and 4.2.1).

LBM

This is one of the experiments where the vehicle crossed the x-axis. Between ping 74 and ping 75 is four ping missing and between ping 75 and ping 76 is one ping missing. The effective bandwidth is 25.6 kHz. The only target illuminated is the T-target. The nearest beacon is

detected in all 200 pings. However the second beacon is at approximately the same range as the two-way echoes from the closest targets. Therefore it is only distinguishable for a few pings namely 1-12 and 19-51.

From this experiment it is possible to do 1-beacon positioning. Autopositiong is possible for any part of the track that does not include ping 74-76. Since the T-target is illuminated, the effective bandwidth is wide enough and positioning is possible it should be possible to generate a SAS image. However strong seabed echoes and an overlapping beacon might obscure this weakly reflecting target.

LAP

There is one ping missing between ping 87 and 88, 134 and 135 and 140 and 141. Two pings are missing between ping 135 and 136. Finally three pings are missing between ping 88 and 89. The effective bandwidth is 17.6 kHz. The beacons are detected for all 200 pings. The ROV stopped halfway so data from the second part of the track is not useable. Data is recorded up to 50m range and since the targets are positioned at approximately that distance they are only covered in the beginning of the track. So even though all targets are illuminated in the middle of the track SAS images can not be generated there. In the beginning of the track the targets are in range and illuminated for a few pings. The T-target is not illuminated at all in the beginning of the track. In this experiment the sampling frequency is increased and the PRF decreased. However, the ROV was driven at its standard operational speed, resulting in a too high movement per ping. This introduces multiple image artifacts and remove the possibility of DPCA autopositioning.

Since both beacons were detected it is possible to do 2-beacon positioning (and obviously also 1-beacon positioning). It should be possible to generate SAS images of the ladder and the mine-like objects for a few pings at the beginning of the track since they are illuminated, the bandwidth is wide enough and positioning is possible. However the high speed will decrease performance.

4.1.2 Calibration

The kernel sets used in the software are computed from stored replicas of the transmitter pulses. The pulses for which replicas are needed are the beacon-pulse for positioning and the M- and P-pulses sent out for imaging purposes.

The first calibration attempt failed. A constant incident angle error of 40 degrees due to two compasses disturbing each other was discovered. However this was discovered quickly and a recalibration took place the next day.

The replicas were taken with the receiver at a water depth of 3m and a distance of 18m from the transmitter, which also was located at a depth of 3m. The seafloor was at 4.9m. For each replica five pings were taken in the boresight direction and two other fixed angles. The ping, with the smallest estimated incidence angle, was then used for calibration. In Table 4.1 the fixed angles are called straight, left and right. They correspond to an intended -20, 0, +20 degrees of rotation of PLUMS vs. boresight respectively. Acceptable incident angles for each signal could be found, but a twenty-degree difference (~0.35 radians) were not fully obtained.

Figures 4.1, 4.4 and 4.5 show polar images of the transmitter, generated from the straightest kernel for each pulse.

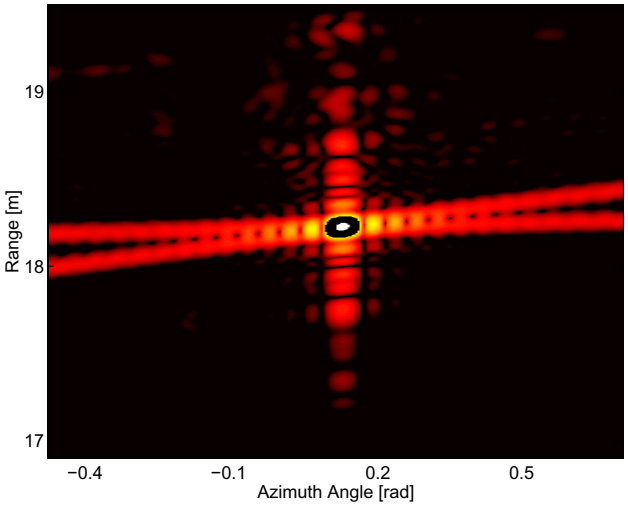

Figure 4.1: Calibration dB image of the transmitter for the beacon-pulse.

Table 4.1: Incident angles during the calibration experiment. Straight, left and right corresponds to the nominal -20, 0, +20 degrees of rotation of PLUMS vs. boresight respectively. The pings used for calibration are marked.

Pulse	Main angle	Ping number	Incidence angle (radians)
Beacon:	Straight	1	-0.212654
	Straight	2	-0.211707
	Straight	3	-0.211283
	Straight	4	-0.211353
	Straight	5	-0.211513
	Left	1	0.116046
	Left	2	0.116041
	Left	3	0.115607
	Left	4	0.115205
	Left	*5*	*0.114185*
	Right	1	-0.367195
	Right	2	-0.367454
	Right	3	-0.367608
	Right	4	-0.367876
	Right	5	-0.368585
M:	Straight	1	0.056862
	Straight	2	0.057719
	Straight	3	0.057279
	Straight	4	0.056998
	Straight	5	0.057143
	Left	*1*	*0.007547*
	Left	2	0.007727
	Left	3	0.007913
	Left	4	0.008264
	Left	5	0.008843
	Right	1	-0.387020
	Right	2	-0.385425
	Right	3	-0.383224
	Right	4	-0.381914
	Right	5	-0.381823
P:	Straight	1	-0.217501
	Straight	2	-0.217767
	Straight	3	-0.218329
	Straight	4	-0.217266
	Straight	5	-0.217419
	Left	1	-0.019948
	Left	2	-0.020119
	Left	*3*	*-0.019245*
	Left	4	-0.020350
	Left	5	-0.020514
	Right	1	-0.576787
	Right	2	-0.576921
	Right	3	-0.577492
	Right	4	-0.577717
	Right	5	-0.579388

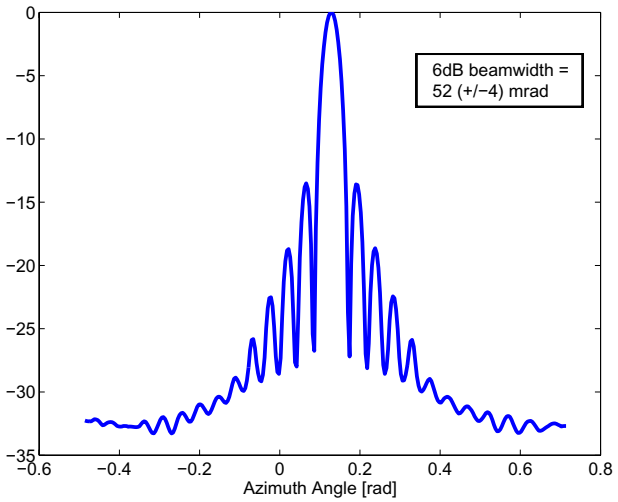

Figure 4.2a: Azimuth beam pattern for the beacon-pulse.

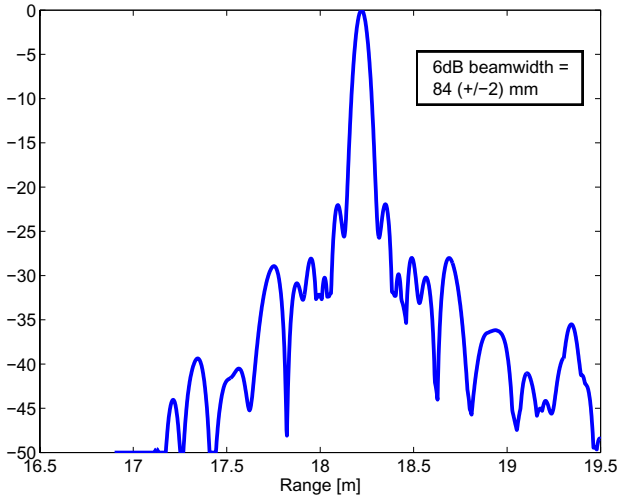

Figure 4.2b: Beacon pulse range beampattern.

If the transmitter could be considered a point source, the half-power beamwidth is an estimate of resolution. Obviously objects less separated than the beamwidth could not be distinguishable. The beacon pulse range resolution was determined to be 84 (+/-2) mm from Figure 4.2b. The beacon pulse azimuth beamwidth is 52 (+/-4) mrad. The beampattern is shown in Figure 4.2a. Beacon positioning is thereby limited by this accuracy.

Physical aperture image resolution is limited by the beamwidth of the two pulses used. The M-pulse gives a resolution of 58 (+/-2) mm in range and 52 (+/-4) mrad

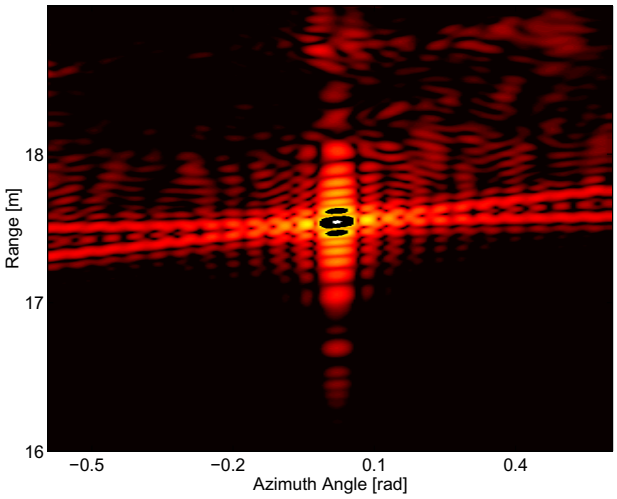

4.3: Calibration dB image of the transmitter for the M-pulse.

in azimuth. The beampatterns are shown in Figures 4.4a and 4.4b. The P-pulse gives less range resolution but similar azimuth resolution. Figure 4.6b shows the range beampattern and the half-power beamwidth is 72 (+/-2) mm. Finally the azimuth beampattern is shown in Figure 4.6a and the corresponding azimuth resolution is determined as 48 (+/-4) mrad.

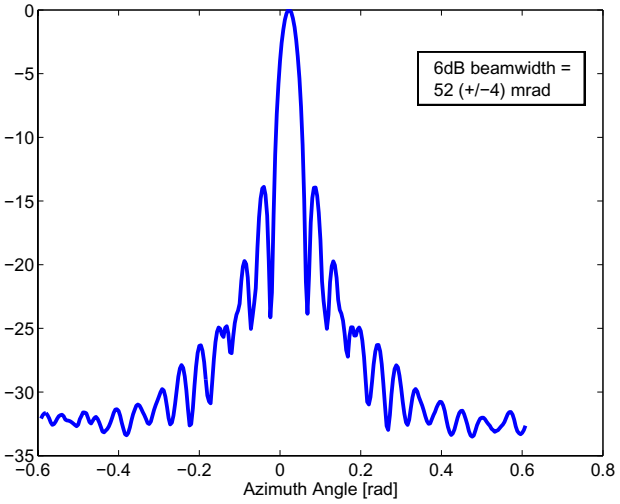

Figure 4.4a: Azimuth beampattern for the M-pulse.

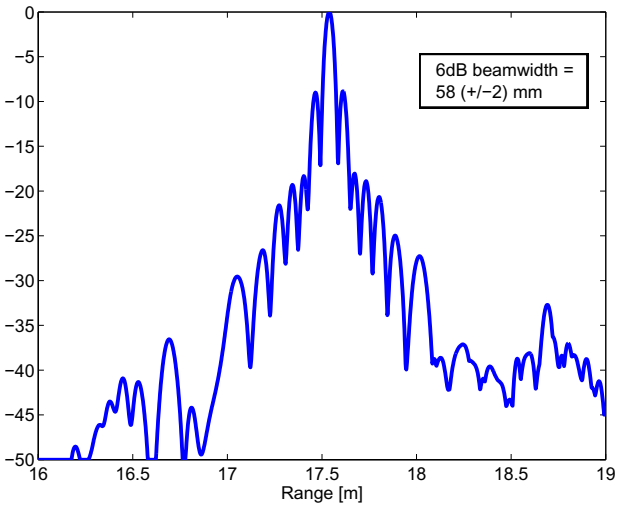

Figure 4.4b: Range beampattern for the M-pulse.

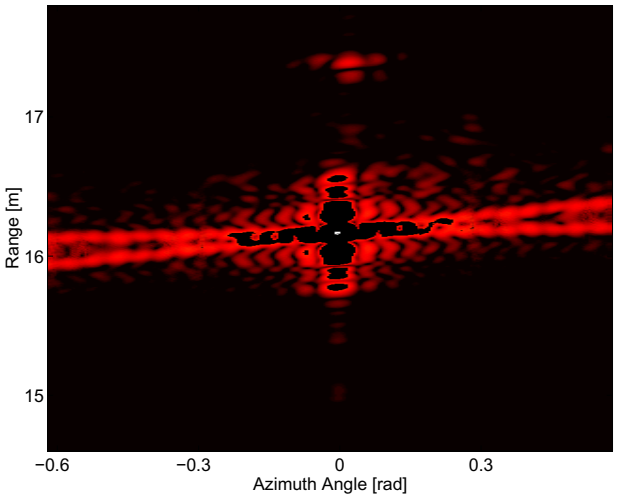

Figure 4.5: Calibration dB image of the transmitter for the P-pulse.

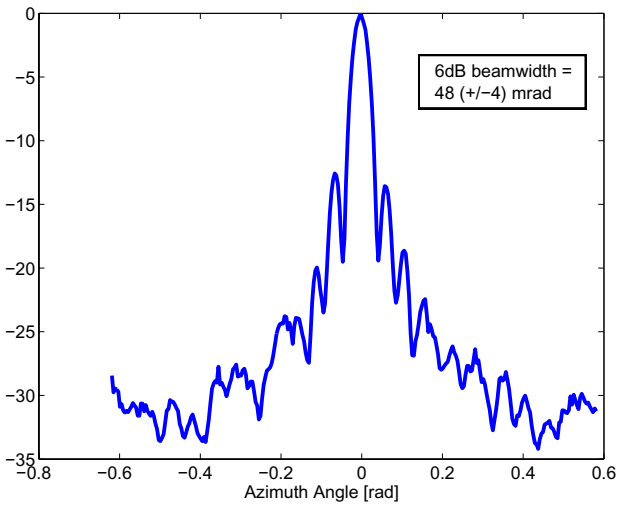

Figure 4.6a: Azimuth beam pattern for the P-pulse.

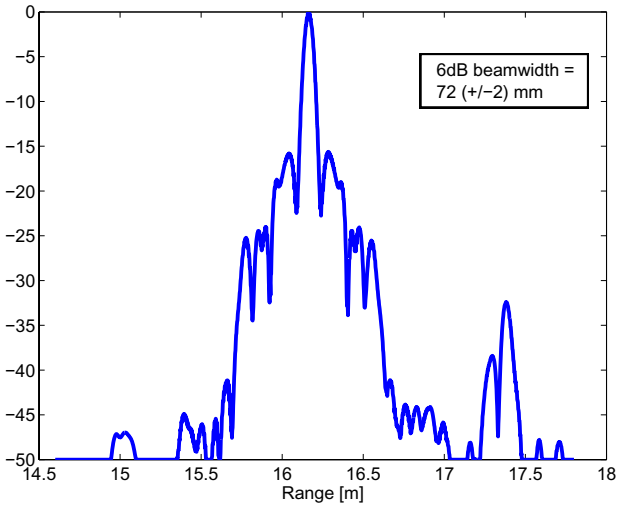

Figure 4.6b: Range beampattern for the P-pulse.

4.1.3 Travel time variability

Two beacons were placed on the seafloor just outside the target area. They could act both as transmitters or receivers. Since they were stationary, the pair were useful for studies of propagation variability in the water column. Two data sets were collected, with each beacon acting as transmitter and the other as receiver. Travel times between the beacons were collected from 1135 pings for each case, during 2 minutes. Mean values and standard deviations are given in Table 4.2 below. Figure 4.7 shows travel time (with mean value subtracted) for all pings. No trend towards shorter or longer travel times can be discerned over the timescale (2 minutes) of the experiments. However, there is a large variance in the data. This means that the distance between the beacons can not be resolved better than the standard deviations imply - of the order of 10 mm, if c is assumed to be 1430 m/s. There is also a difference between the travel times recorded in the two directions of the same order as the standard deviations within the data.

Table 4.2: Travel-times between the two beacons.

Transmitter	Receiver	Traveltime	
		mean [ms]	σ [ms]
Beacon 1	Beacon 2	24.230850	0.005904
Beacon 2	Beacon 1	24.222240	0.008210

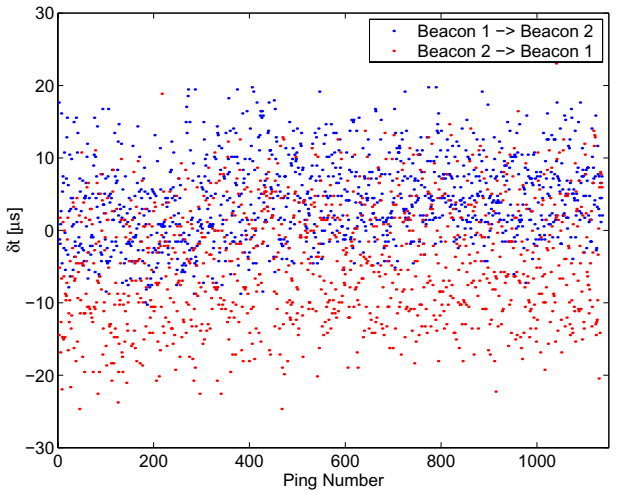

Figure 4.7: Travel-times between the two beacons.

4.1.4 Positioning

As mentioned in Section 2.3, heading can be obtained from 1-beacon positioning if initial heading and platform speed are known. Here the speed is taken as the mean value of the estimated speed for the pings where two good beacons are present. For the LBM experiment, a mean speed of 0.30m/s was extimated from pings 1-10 and 20-40. In Figure 4.8 a comparison is made between heading from the mean velocity and the PLUMS data. This comparison leads to the conclusion that there is a time delay of about 28 pings. This delay is the synchronisation error between the different computer-clocks used in the separate systems, and is compensated by delaying the PLUMS data.

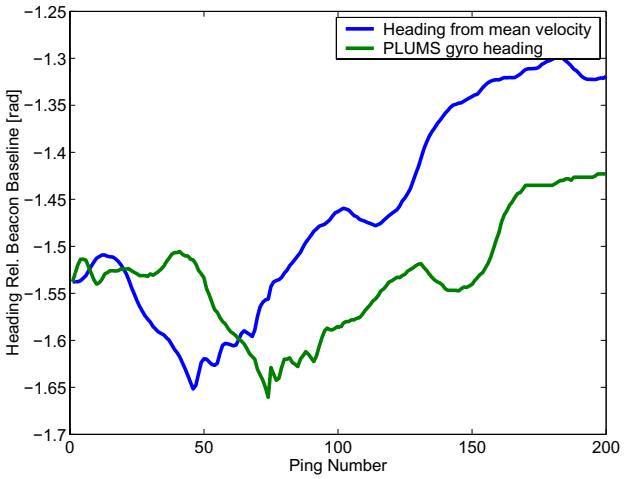

Figure 4.8: Comparison between heading obtained from the average speed and the PLUMS recorded heading. The heading is defined positive counter clockwise from the x-axis in the beacon coordinate system.

After synchronizing the data, the tracks obtained for the LBM experiment using the two approaches are given in Figure 4.9. It appears from the figure that the mean speed based on the chosen pings is a bad representation of the mean speed for the whole track, i.e. after half the track, the alternative track estimates diverge.

For the LAP experiment there exists range and angle estimates for ping one to eighty for both beacons, hereafter PLUMS seemed to stop, why no useful estimates could be done. From these data 2-beacon triangulation is done and the obtained track is compared with the 1-beacon approaches in Figure 4.10. The speed is taken as the average over pings 1 to 70 (0.31 m/s).

As seen from the figure the incidence-heading approach corresponds better with the 2-beacon track than the mean speed approach. In subsequent processing, when only one good beacon is available, the incidence-angle track is therefore used, while the mean speed method is primarily used to determine the synchronization error.

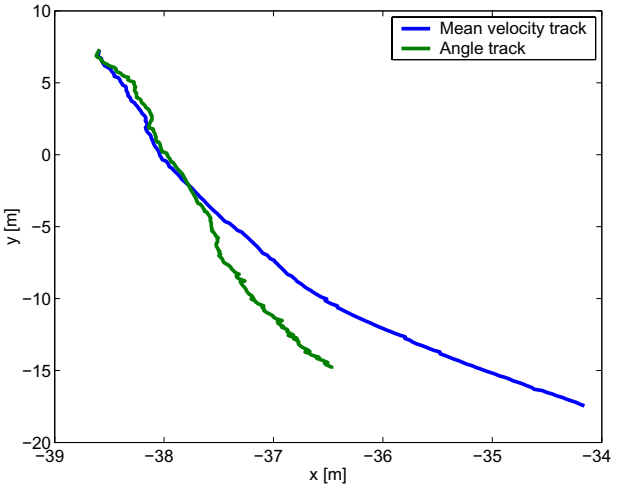

Figure 4.9: Comparison the tracks obtained from the mean speed and from the incidence and heading angles.

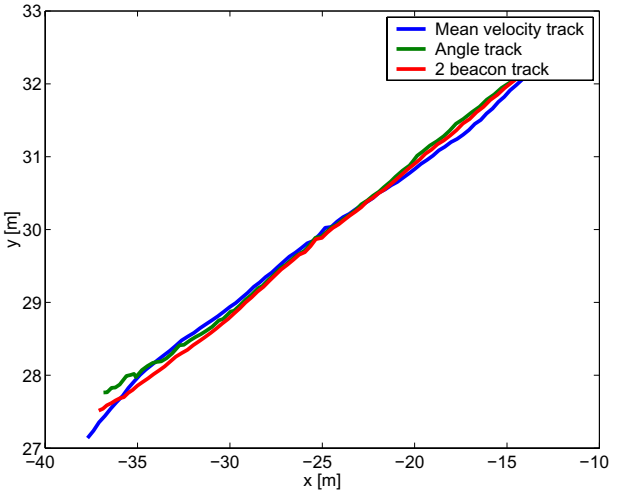

Figure 4.10: Comparison of tracks obtained with 1- and 2-beacon positioning.

4.1.5 Side-scan

Sidescan images were generated by beamforming the redeiver array in the boresight direction, and simply stacking the consecutive echoes. The receiver array is 32 wavelengths long at mid-frequency, so angular resolution is just under two degrees. This is worse than a commercial sidescan sonar, because there is no azimuth directivity on transmission. Figure 4.11 shows a sidescan image from the LBM run. The arc at about 10m range is the closest beacon. The other beacon is visible for the first 40 pings at about 28 m and is then covered by two-way bottom echoes from the SAS transmitter. Figure 4.12 shows a sidescan image of the most illuminated area from the LBM run. The most distant beacon is noticeable but no targets.

Figure 4.13 shows a sidescan image from the LAP run. Both beacons are visible and one bottom or surface reflection from each beacon is identifiable. It is obvious that PLUMS stopped or at least moved extremely slow after half the run. The limiting range of recorded data at 50m is also apparent. Figure 4.14 shows a sidescan image of the most illuminated area from the LAP run. No targets are visible.

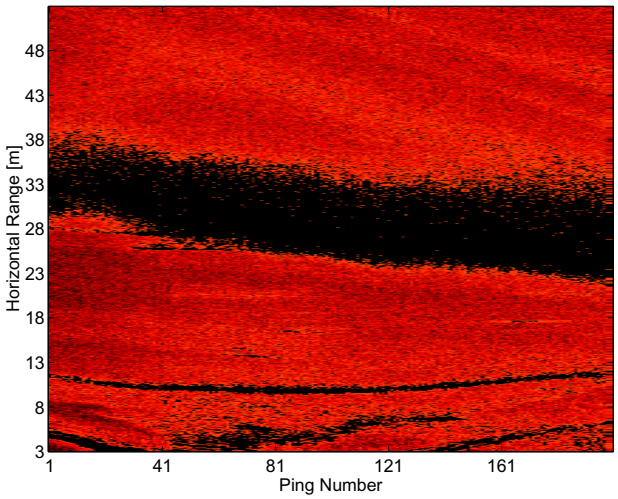

Figure 4.11: LBM Sidescan image.

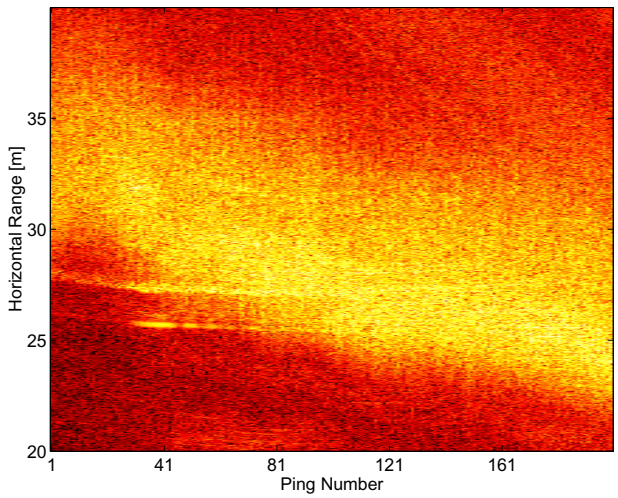

Figure 4.12: LBM Sidescan image over the most illuminated area.

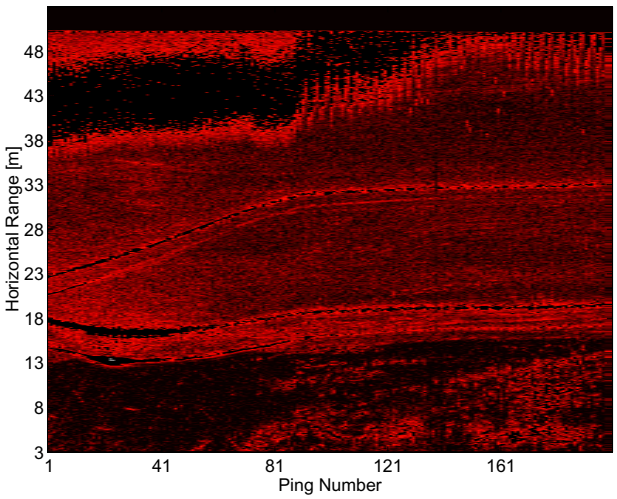

Figure 4.13: LAP Sidescan image.

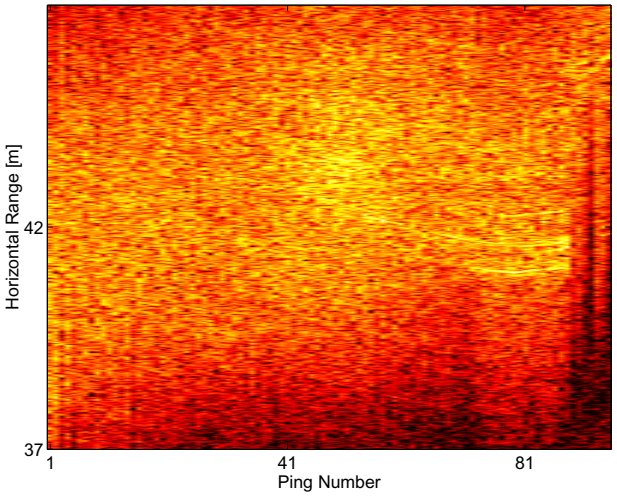

Figure 4.14: LAP Sidescan image over the most illuminated area.

4.2 Autopositioning and SAS imaging

The experiments were affected by many different problems. Data is totally unusable from several of the runs. However a determined attempt has been made to extract useful results from the LAP and LBM experiments. 2-beacon positioning only seems to have worked well in the LAP experiment. Unfortunately PLUMS speed was around 36 cm movement between pings, which is 50% higher than the speed allowed for SAS imaging, and three times the maximum speed for DPCA correlation autopositioning. PPP was tried on one of the targets, but the corruption due to excessive speed makes it very difficult to assess performance (Figure 4.25b). It is easy to find three quite strong targets in the LAP data. However in this experiment, sonar echoes were only recorded out to a range of 50 m, so each target is only visible for a short section of the track.

The LBM experiment was carried out at a reasonable speed, 10.5 cm ping-to-ping displacement of the platform. Unfortunately 2-beacon positioning either failed or was very inaccurate for most of the track, due to faulty positioning of the beacons. This meant starting with no reliable knowledge of heading, since Djupviken had shown that the recorded PLUMS heading was unreliable. Thus LBM became the first field experiment which required determination of three parameters by autopositioning, heading and along and across track movements. It was extremely valuable that new programs for heading estimation has been developed in time for the Älvsnabben experiment. These *autoheading* programs are described in Section 2.4

With knowledge of heading, it was possible to carry out 1-beacon positioning which meant that it was possible to predict the target locations in relation to the PLUMS track. Much time and effort has been devoted to detecting, let alone identifying, any objects in these locations but without success. However some smaller objects have been detected at closer range. Presence of point-like targets made it possible to investigate three-parameter autopositioning with a degree of success. This work is still in progress, and the experiment has been extremely valuable, even if the images appear uninteresting from a mine-detection viewpoint.

The geometry of correlation autopositioning is very sensitive to the elevation angle of the returning sonar echoes. In the Älvsnabben environment, this elevation angle was very dependant on sonar range. It is possible to autoposition on a chosen area without accurate knowledge of the depth, but the estimated track corrections will then only apply to this local area. Hence autopositioning has to be carried out separately for each individual target location, using an "image frame" fixed to the seabed.

Mean displacement gives the along-bearing displacement between the two DPCA's, whereas slope gives the difference between ping-to-ping array rotation and the rotation predicted in the navigation file. Typical displacement estimates are shown in Figure 4.15.

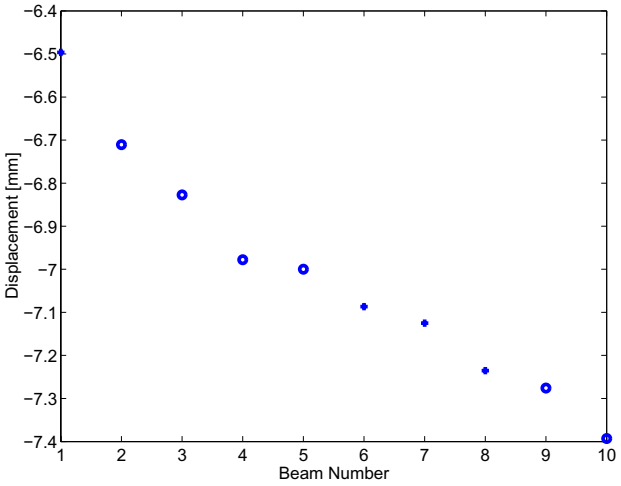

Figure 4.15: Autopositioning displacement estimates using echo correlation.

The location of the centre of the frame on the seabed is very important. With target autopositiong the frame is deliberately chosen for the purpose of getting as good navigation values as possible for this particular region of the seabed. The intermediate FFBP image is quite sparse, particularly in the y direction, in order to obtain long sample sequences for good correlation. A typical image is 27x3. Correlation of the two images then gives 81 possible displacement values. However not all correlations are useful, as can be seen from Figure 4.16. The displacement estimates are very subject to ½λ ambiguities, as well as other outliers. The correlation displacements are weighted by a combination of ccf and cross-power. The "heavier" pixels are marked with crosses in the diagram, and the colour-coding shows that all of these belong to the same range bracket.

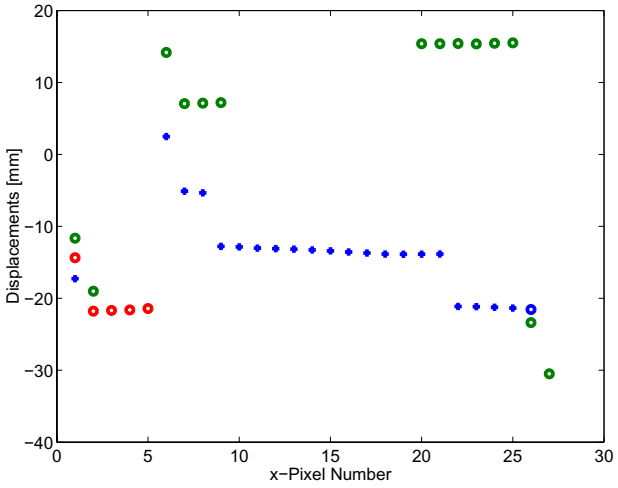

Figure 4.16: Autopositiong displacement estimates using image correlation before ambiguity correction.

After ambiguity correction, the plot becomes:

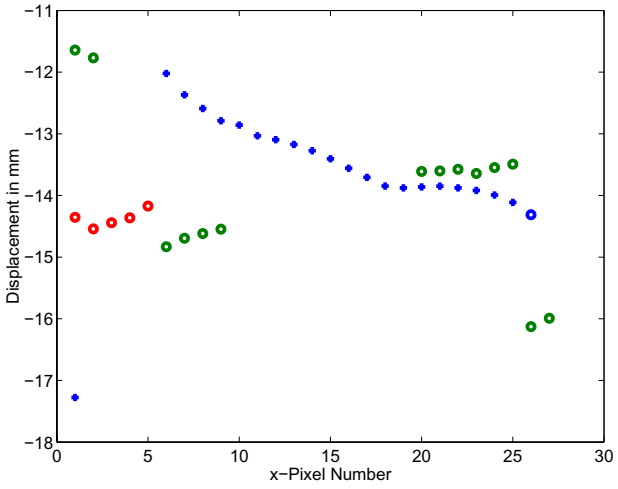

Figure 4.17: Autopositioning displacement estimates using image correlation after ambiguity correction.

4.2.1 LBM Experiment

Autopositioning was carried out in parallel with attempts to improve beacon positioning. The first guesstimate at a navigation file assumed zero y displacement, zero heading angle with respect to the x-axis, and a constant forward speed of 15 cm/ping. This was based on the PLUMS operator's assessment. Pitch, roll, and depth values were taken from the PLUMS recording.

The first step was to run *autoecho* using a moving image area and broadside echoes over the whole 200 pings. Correlation levels were investigated for a range of subarray lengths. Highest DPCA correlations were obtained for a subarray length of 18 channels, giving a separation of 10.5 cm between the centres of leading and trailing subarrays. This suggested a lower platform speed around 10.5 cm/ping.

Figure 4.18 below compares *autoecho* heading with PLUMS compass heading. Two things stand out. Firstly the shapes of the two curves agree extremely well, apart from a delay of 28 pings between the two records. This pointed to a large synchronization error between the recorded PLUMS data and the sonar data. Such a large error seemed unlikely but was subsequently confirmed by 1-beacon positioning (Section 4.1.4). Secondly there seems to be a significant bias in the ping-to-ping displacements.

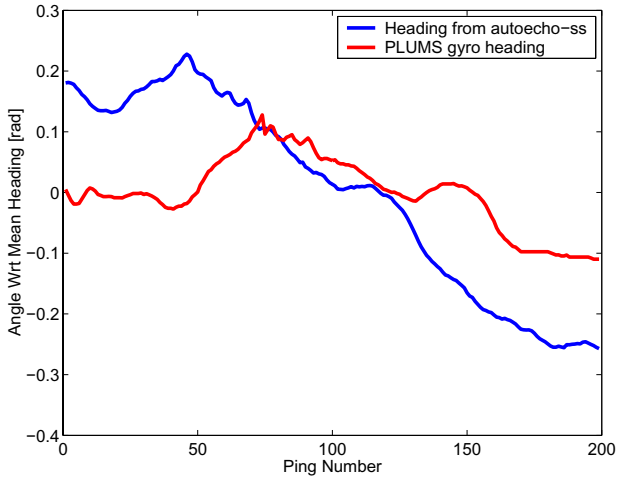

Figure 4.18: Comparison between Autoecho heading and PLUMS compass heading.

Comparison of the delayed graphs (Figure 4.19) gives a bias error around 2.4 mrad/ping, though the actual value depends considerably on the region used for comparison. A bias error of this size in the compass record is extremely unlikely, so we considered the possibility of such a bias in the autopositioning estimate. Extensive simulation studies were carried out simulat-

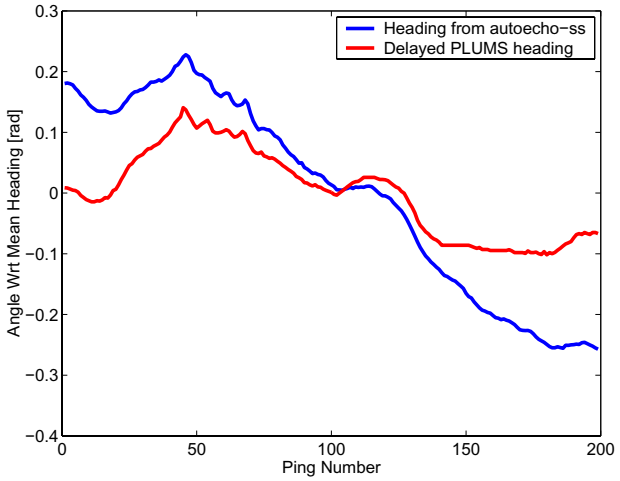

Figure 4.19: Comparison between Autoecho heading and delayed PLUMS compass heading.

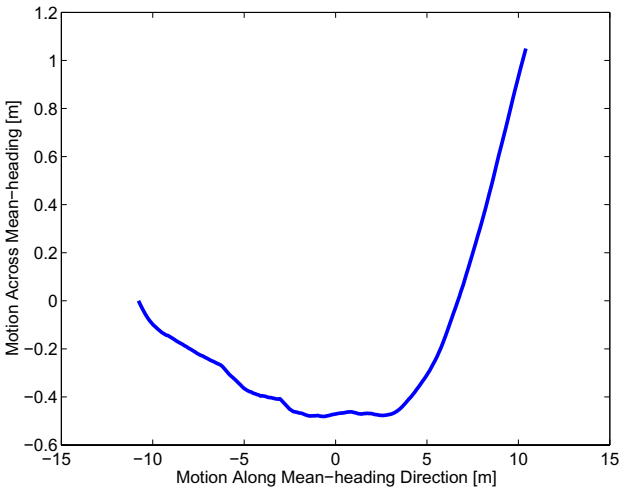

Figure 4.20: LBM track estimated by autecho-ss and autoimage-ss.

ing the depth, pitch, and roll conditions of the LBM experiment. However bias errors were of the order of 0.01 mrad, far too small to account for the errors observed. Now the DAIM receiver array is split into two 16-channel physical subarrays. These are mounted in a holder, which allows the receiver configuration to be changed for different purposes. Any relative movement of the two physical subarrays after calibration would immediately introduce a bias error. A 2 mrad change of angle between the subarrays could certainly occur unless care was taken to avoid it. Hence this is the likely cause of the problem. The bias problem was only apparent after processing had started, and is not a fundamental problem with the autopositioning method. However it added a further difficulty to the actual autopositioning processing.

The pitch, depth, and roll values in the navigation file were now corrected for the 28 ping delay, and the whole Autoecho operation repeated. It was important to smooth these depth and attitude values in order to avoid large spikes in the heading record. Autoecho and Autoimage were then run in turn to obtain the track estimate shown in Figure 4.20. Uncertainty about the bias error affects the track curvature considerably.

The autopositioned track was generated in track coordinates, a coordinate system with origin at the middle of the track, and with x-axis aligned with mean heading. The expected target locations were not available in this frame of reference. However the 1-beacon track was generated in a coordinate system for which target locations were known. The two tracks were then compared, allowing target locations to be converted to track coordinates. One interesting strategy was to use the T-target hydrophone recordings giving the propagation time from transmitter to target-hydrophone for each ping along the track. Triangulation of these delay times should indicate the location of the T-target. This method did indeed give an expected location, but in spite of a determined search of the area, no trace of the T-target was detected.

However some other objects were detected on the seabed at shorter ranges. A first image of one of these is shown in Figure 4.21a. This looked interesting, so attempts were made to improve the image quality. The

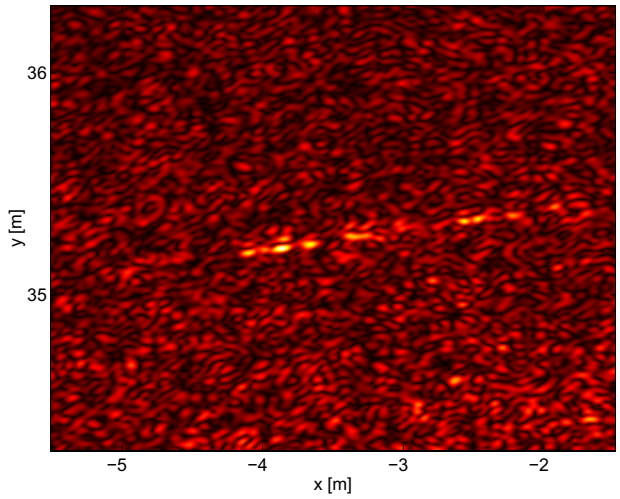

Figure 4.21a: A first image of a short-range target.

"wings" either side of the bright spot do not resemble sidelobes, but there was a suspicion that they might be due to angle errors.

After careful autopositioning using seabed echoes in the target region, the result shown in Figure 4.21b was achieved. This shows very high spatial resolution with low sidelobe levels. The corrected navigation file is only local, as shown in Figure 4.22 where a second point-like target at different range and depth is imaged. 32 pings were used to generate both images, corresponding to a synthetic aperture length of 3.4 m

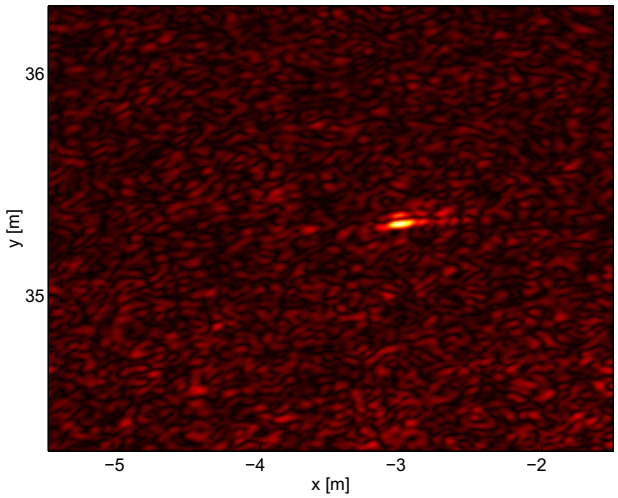

Figure 4.21b: Improved image using autopositioning.

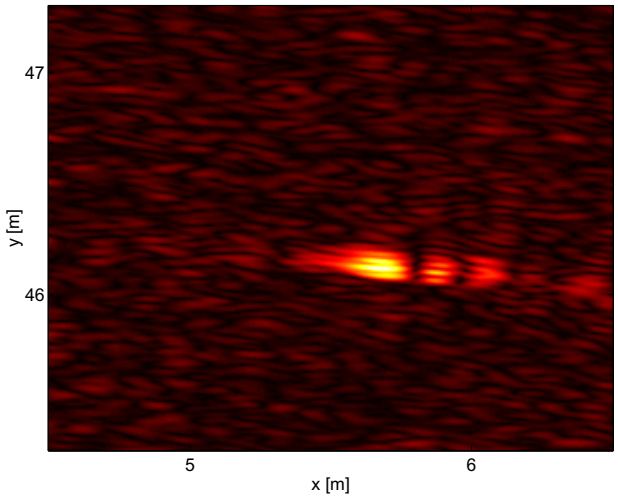

Figure 4.22: An image of point-like target at different range and depth compared with the object in Figure 4.21 using the navigation file that improved Figure 4.21.

4.2.2 LAP Experiment

For this experiment, the PLUMS track was well oriented with respect to the beacons so good beacon positioning was possible for the whole track. Figure 4.23 below shows along-heading platform speed given by beacon positioning.

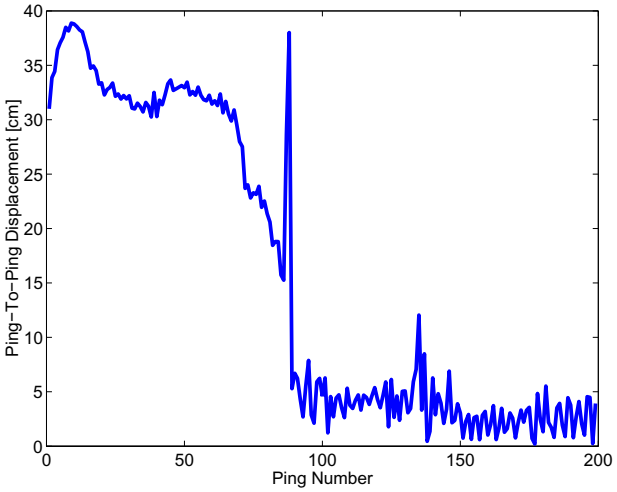

Figure 4.23: Along-heading platform speed given by beacon positioning for the LAP run.

For the first half of the run, platform speed was too high, while for the second half the vehicle was almost stationary. The maximum speed for SAS imaging without azimuthal ambiguity is 24 cm/ping, i.e. half the array length. For most of the early part of the run, the speed was well in excess of this limit. Between pings 70 and 85 the speed drops down to an acceptable value. The maximum speed for DPCA autopositioning is around 12 cm/ping, so correlation autopositioning was only possible after ping 90. However all the targets were located before the start of the track, and the maximum sonar range was limited to about 50 m, because of the high sampling rate used in this experiment. The narrow transmitter elevation beam angle also restricted target imaging. The combined effect of these restrictions is shown in Figure 4.24. However, this diagram is based on nominal target locations, so the limiting positions are only approximate.

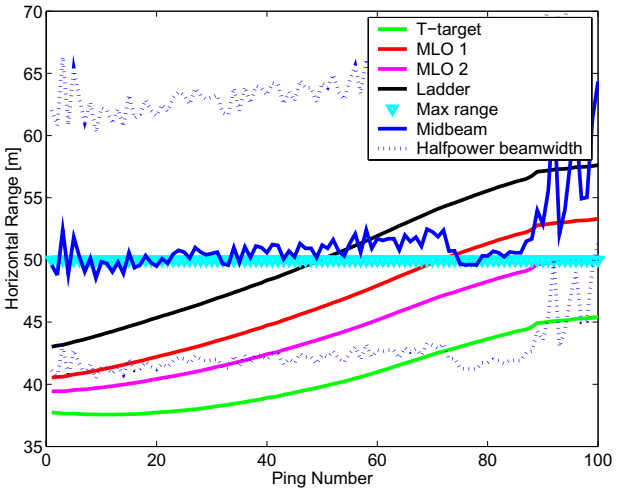

Figure 4.24: Illuminated ranges and target positions for the LAP experiment.

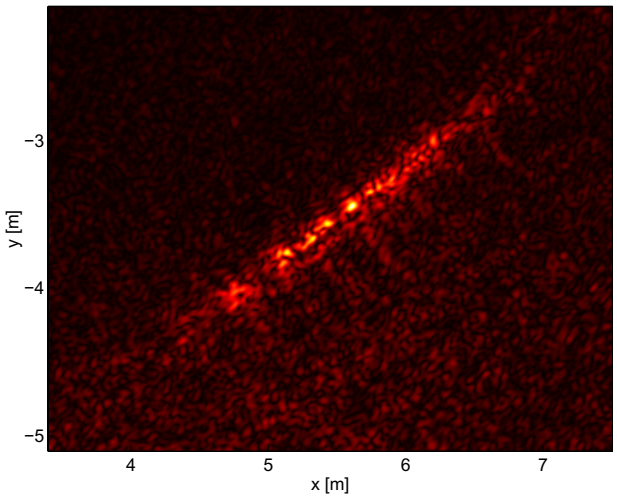

Figure 4.25a: SAS images of a strong target.

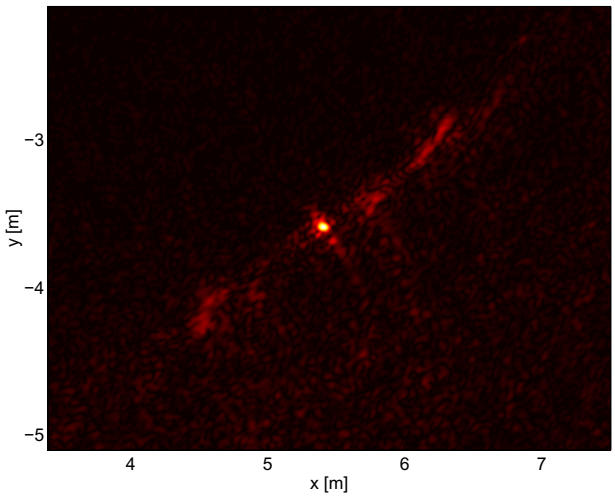

Figure 4.25b: Improved image using PPP.

Figure 4.25a below shows an image generated by a strong target using pings 10-30 at the beginning of the track. The location of this object was nearest to the expected step-target location. Although there seems to be interesting structure, this is parallel to the point-spread function and therefore suspect. The structure is likely to be caused by some combination of azimuthal ambiguity due to excessive platform speed, angle errors, and sidelobes arising from phase incoherence. There are no restrictions on platform speed for principal point positioning. The main requirement is an isolated strong reflector. Figure 4.25b shows the same scene after PPP, with the principal point enhanced.

A systematic search of the area for other targets was made by generating SAS images of sections of the scene. No further targets were found in this way. An alternative method of target detection using stacked aligned echoes is illustrated in Figure 4.26 below. The targets appear as lineations in the plot of echo amplitude. The range and angle of these lineations can easily be used to determine target locations. Moreover the strength and weakness of the lines show which pings insonify the target. In the particular image below, the nearly vertical line shows the step-target track. There are at least three other object tracks visible in this image. However when these locations were imaged, no obvious target appeared, presumably because of destructive phase interference along the synthetic aperture.

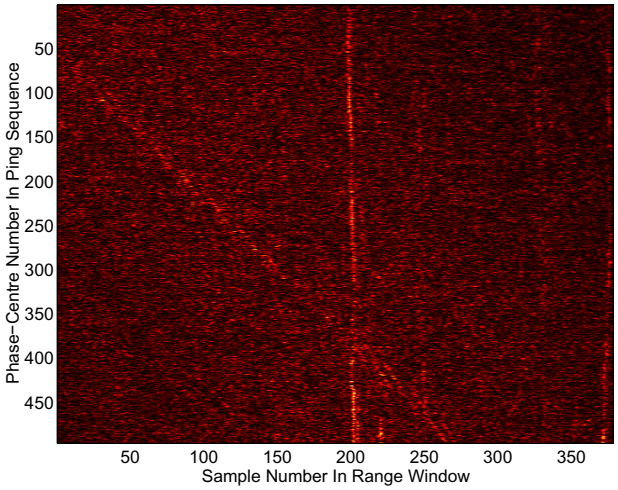

Figure 4.26: Stacked aligned echoes from the LAP experiment showing four targets

4.3 Discussion

The results from this processing may seem disappointing compared with Djupviken. However it should be remembered that the defined task was to identify detected targets. At Älvsnabben, the hardest problem has been to detect targets buried in strong seabed reverberation. The targets were also not properly illuminated.

The work on correlation autopositioning has advanced considerably since Djupviken. The LBM experiment has been invaluable in providing good experimental data. It was an important success to generate a good SAS image of a point-like target, starting without knowledge of track, speed or heading. However the processing methods need to be developed further to handle the greater number of unknowns. One could conclude that although autopositioning is possible with unknown heading, it is a great deal easier when heading is known.

5 Summary and conclusions

5.1 Experiences of the field test

The field experiment at Älvsnabben was a valuable test of our methods in a difficult environment. The earlier Djupviken experiment showed that easily detected targets could be identified with the aid of Synthetic Aperture Sonar. It also showed that the autopositioning algorithms using strong target echoes succeeded in determining the ROV track with the required accuracy. However the algorithms relied on good heading information. In the Djupviken experiment, this heading information came from beacon positioning, although it would normally be obtained from the vehicle's own navigation system.

The Älvsnabben experiment was designed to investigate performance with stronger seabed reverberation and a sloping seabed. Imaging was also made at shorter range. As a result the transmitter footprint was decreased. The sonar transmitter was therefore modified to give a wider elevation lobe pattern. However the footprint was still small which meant that the transmitter had to point in almost exactly the right direction to illuminate the targets properly.

Unfortunately the targets were not correctly set out in relation to the ROV track, which meant that they were only intermittently insonified, or not at all. In these circumstances it proved extremely difficult to detect any target, let alone identify it. The ROV tracks were also incorrectly set out in relation to the underwater beacons, so beacon positioning failed much of the time. There were other problems due to the use of equipment designed for other purposes which made measurements and subsequent analysis extremely complicated. Because of equipment incompatibility, some measurements had to be done by hand. This led to poor synchronisation between the sonar system and the ROV's own attitude and heading recorder.

From a processing viewpoint the experiment was very interesting. The new FFBP (Fast Factored Back Projection) developed by FOI, Linköping for ultra-wideband SAR, was converted to SAS and used to process the experimental results faster than was previously possible. There are plans to make FFBP run even faster.

Very good echoes were obtained from the seabed most of the time. These were used to extend the autopositioning algorithms to determine heading as well as track. The new algorithms exploit FFBP imaging. The lack of a commercial-grade navigation system on the ROV, together with the general failure of beacon positioning, makes it difficult to evaluate autopositioning accuracy, but good SAS images were generated of point-like "targets of opportunity".

5.2 Suggestion for improvements and further work

We believe that our SAS algorithms and software now are developed to the stage that a test with a demonstrator is appropriate. Such a system should be equipped with

- positioning system integrating:
  - Doppler log
  - INS
  - Single beacon positioning
  - Correlation autopositioning software
  - PPP
- wideband sonar to a commercial standard, and meeting our specification for SAS operation, including an appropriate digital interface to the recording equipment.
- recording unit which records all relevant data synchronously

With this system it should be possible to arrive at the minimum specification for an operational system, as well as evaluate SAS performance in relation to the accuracy of the on-board navigation system, sonar bandwidth, and other parameters. At the same time, it should be possible to further develop and refine the software towards an operational package.

One problem experienced in the experiments was the slow ROV speed restricted by SAS operation. Removal of this restriction using coded pulses needs to be investigated. Also a larger physical aperture (i.e. a longer antenna) will increase the survey speed.

As demonstrated in the Djupviken experiment such a system will have a resolution of 5 x 5 cm at a 100 m distance.

6. References

1. A. Caiti et al. ”Seafloor Imaging and Toxicity: Assesment of Risks caused by buried waste SITAR”, RTD proposal, 5th Framework Programme of the European Union (2001).

2. J. Pihl and P. Söderberg “Syntetisk apertur sonar i Djupviken”, FOI-R—00-01508-409—SE, ISSN 1104-9154 (2000).

3. G. Shippey, J. Pihl and M. Jönsson “Autopositioning for Wideband Synthetic Aperture Sonar using Fast Factored Back Projection”, Computer-Aided Detection and Computer-Aided Classification Conf., Halifax, Canada (2001).

4. Patent på DPCA.

5. G. A. Shippey, “Simple algorithms for sonar imaging and swath bathymetri with a linear swept frequency (chirp) source”, Int. J. of Imaging and Imaging technology 8, pp. 359-376 (1997).

6. G. A. Shippey, P.Ulriksen and Q.Liu: “Quasi-Narrowband Processing of Wideband Sonar Echoes”, Proc. 4’th European Conf. On Underwater Acoustics, Ed. A.Alippi and G.B.Canelli, pp.63-68, Rome (1998).

7. R. W. Sheriff: “Synthetic Aperture Beamforming With Automatic Phase Compensation For High Frequency Sonars” Proc. IEEE Symp. On AUV Technology, Washington DC, pp 236-245 (1992).

8. M. Soumekh “Synthetic Aperture Radar Signal Processing With Matlab Algorithms”, Wiley-Interscience (1999).

9. L. M. H. Ulander, H. Hellsten, and G. Stenström: “Synthetic-Aperture Radar Processing using Fast Factorised Backprojection”, Proceedings of EUSAR’2000, pp. 753-756, Munich (2000).

10. Q. Liu, O. Kröling, G. Shippey, “Software calibration for a wideband linear receiver array using matchfiltering processing”, Proc. I.O.A., Vol. 21, Part 1, (1999).

11. M. Jönsson, “Positioning in a wideband synthetic aperture sonar field experiment”, FOA-R—00-01575-409—SE, ISSN 1104-9154, (2000).

12. R. O. Schmidt, “A signal subspace approach to multiple emitter location and spectral estimation,” PhD Thesis, Stanford Univ. Stanford CA (1981).

13. “Signal Processing Toolbox User’s Guide”, The Mathworks Inc.

14. G. Shippey, P. Ulriksen and Q. Liu: “Wideband swath bathymetry, SAS autofocus, and underwater navigation fixes: three related problems in echo/image correlation”, Proc. Int. Conf. on Sonar Signal Processing, pp.1-10, Weymouth (1998).

15. A. Bellettino and M. Pinto: “Experimental investigation of synthetic aperture sonar micronavigation”, 5th European Conf. on Underwater Acoustics, Lyon, pp.445-450 (2000).

7. Acknowledgments

The field experiment at Älvsnabben was complicated by many participants. We greatly appreciate the work of Per Söderberg in managing this team. We also would like to thank all participants:
Peter Ulriksen, Dept of Technical Geology, LTH,
Per Gunnarsson, Subvision AB,
Eva Dalberg, Niels Jacobsen, Kjell Lindersson, Marie Olsson, Paul Ström, FOI.

The advice and assistance of Lars Ulander and Mats Pettersson at FOI, Linköping with the SAS implementation of the FFBP algorithm is gratefully appreciated.

Eva Dalberg carried out the propagation time analysis summarised in the Report, while Per Söderberg contributed the description of the experimental environment. Per Morén, is acknowledged for the graphics and for checking the manuscript. Layout and production were expertly done by Eva Norrbrand.